is inserted into N- or C-terminal of purpose gene by PCR or general recombinant method.

3.1.1. Isolation of DBtag Fragment

1. Prepare 100 μL of PCR reaction mixture as the manufacturer's instructions (Takarabio Inc.) by mixing 100 pg/μL of plasmid (pEU-DBtag) and 200 nM of deSP6E02 (5′-GGTGACAC TATAGAACTCACCTATCTCTCTACACA) and DBtag-A (5′-TGGTGGTGGTGGGTGGAAGCCCTGGAAG TACAGGTTCTC), 200 μM of each dNTP, 1.25 units of ExTaq DNA polymerase.
2. Set the mixture to PCR thermocycler for 1 min denaturation at 96°C followed by 25 cycles of amplification: 98°C for 10 s, 55°C for 30 s, and 72°C for 1 min.
3. Incubate the amplified product with exonuclease I (1 U/10 μL reaction mixture) for 30 min at 37°C, and then treat for 30 min at 80°C (see Note 1).
4. Purify them with a PCR product purification kit.
5. Check concentration of the DBtag fragment.

3.1.2. Construction of DNA Template for DBtag Protein by Split-PCR

1. Prepare 50 μL of a first PCR reaction mixture by mixing 3 ng of plasmid or 3 μL of *Escherichia coli* (overnight culture) as template, 200 μM each of dNTP, 1.5 units of ExTaq DNA polymerase, 10 nM of target protein-specific primer (5′-CCACCCACCACCACCAatgnnnnnnnnnnnnnnnn; uppercase and lowercase indicate common sequence and the 5′-coding region of the target gene, respectively) and AODA2306 primer (5′-AGCGTCAGACCCCGTAGAAA, this primer is designed on pUC Ori sequence), and the buffer supplied by the manufacturer.
2. Set the first mixture to PCR thermocycler for 4 min denaturation at 94°C followed by 30 cycles of amplification: 98°C for 10 s, 55°C for 30 s, and 72°C for 5 min depending on the length of gene (1 kb per min).
3. Prepare 50 μL of a second PCR reaction mixture by mixing 5 μL of the first PCR product (without any purification) above as template, 200 μM each of dNTP, 1.5 units of ExTaq DNA polymerase, 100 nM SPu primer (5′-GCGTAG CATTTAGGTGACACT), 100 nM AODA2303 primer (5′-GTCAGACCCCGTAGAAAAGA, this primer is designed on pUC Ori sequence), and 2 nM DBtag fragment and the buffer supplied by the manufacturer.
4. Set the second PCR mixture to PCR thermocycler for 1 min denaturation at 98°C followed by 30 cycles of amplification: 98°C for 10 s, 55°C for 30 s, and 72°C for 5 min depending on the length of gene (1 kb per min).

5. Check the DNA template production by agarose electrophoresis (see Note 2).

3.2. DBtag Protein Production by Wheat Cell-Free System

We use bilayer method for protein production by the cell-free system (10). In principle, exchange of substrates and dilution of by-products take place between translation mix and TSB by expansion of translation mix.

3.2.1. Preparation of mRNA

1. Prepare 30 μL of transcription reaction by mixing 3 μL of the PCR mix (without any purification) as template, 6 μL of 5× TB, 3 μL of NTPs mix, 25 units of SP6 RNA polymerase, and 25 units of RNasin with Milli-Q water.
2. Incubate the reaction mixture at 37°C for 3 h.
3. Add 3 volumes of Milli-Q water, 1/7.5 vol. of 7.5 M ammonium acetate, and 2.5 vol. of ~99% EtOH, and keep on ice for 10 min after mixing well.
4. Centrifuge the mixture (20,000*g*; 5 min) and discard the supernatant.
5. Wash the pellet with 500 μL of 70% ethanol and then spin for 5 min at 20,000*g*.
6. Dissolve the mRNA pellet in 10 μL of Milli-Q water.

3.2.2. Preparation of DBtagged Proteins by Wheat Cell-Free Protein Production

1. Prepare 25 μL of translational reaction mixture by combining 6.3 μL of wheat embryo extract (final conc. 60 OD/mL), 1 μL of 10 mg/mL creatine kinase, 4.5 μL of 4× TSB, and 10 μL of the dissolved mRNA above.
2. Add 125 μL of 1× TSB in the U-shaped titer plate well.
3. Carefully place 25 μL of the reaction mixture at the bottom of titer plate well.
4. Place a coverlet on the plate and then wrap with the Saran Wrap to avoid evaporation.
5. Keep the plate in an incubator at 17°C for 16 h without shaking.

3.3. Generation of Protein Microarray Using DBtag Protein

We designed a new microplate that carries a thin layer of agarose gel containing DNA (agarose/DNA microplate) to immobilize and purify the DBtagged proteins on the microplate (Fig. 7.1b). Non-DBtagged proteins are washed out (Fig. 7.1c).

3.3.1. Preparation of Agarose/DNA Microplate

1. Melt 0.2% agarose gel in 1× TMD buffer, and subsequently add 1 mg/mL (final concentration) salmon sperm DNA.
2. Before the gel is solidified, spread 600 or 400 μL of the agarose gel/DNA mixture above on a slide glass or a Lab-Tek II Chamber slide, respectively, to form a thin layer (0.5–0.6 mm) (see Note 3).

3.3.2. Preparation of Protein Microarray on Agarose/DNA Microplate

1. Spot approximately 10 nL of each translational mixture per 0.2 mm^2 (~500 μm in diameter) on the agarose/DNA-coated glass plate by using pin-type spotter according to the instruction manual (see Note 4).
2. Soak the microplate in the wash buffer for 15 min.
3. Use immediately for assay (see Note 5).

3.4. Functional Analysis of DBtagged Protein on Agarose/DNA Microplate (see Note 5*)*

Using this new protein microarray, we demonstrate (a) the autophosphorylation activity of the fusion human protein kinases (Subheading 3.4.1. and Fig. 7.2a), (b) a protein–protein interaction between UBE2N (Accession no. NM_003348, MGC5063) and UBE2v1 (NM_022442, MGC8586) (Subheading 3.4.2. and Fig. 7.2b), and (c) specific cleavage of the fusion proteins (PAK2, NM_002577) by caspase 3 (Subheading 3.4.3. and Fig. 7.2c).

3.4.1. Inhibition Assay of DBtagged Protein Kinases on Agarose/DNA Microplate

1. Prepare the protein microarray spotting DBtag-fusion protein kinases on the agarose/DNA-coated glass plate as described above.
2. Cover the microplate with a kination solution or inhibitor solution.
3. Incubate for 30 min at 37°C.
4. Soak the microplate in washing buffer for 10 min.
5. Analyze the microplate by Typhoon 9400 imaging system.

3.4.2. Protein–Protein Interaction Analysis Between DBtagged Protein and Biotinylated Protein on Agarose/DNA Microplate

1. Prepare DBtag-UBE2N and biotinylated bls-UBE2V1 proteins by the cell-free system.
2. Mix both proteins with Alexa488-STA (final 10 μg/mL).
3. Incubate for 30 min at 26°C.
4. Spot the mixture on the agarose/DNA-coated glass plate as described above (Subheading 3.3.).
5. Soak the microplate in 1× PBS buffer for 10 min (see Note 6).
6. Analyze the microplate by Typhoon 9400 imaging system.

3.4.3. Caspase Cleavage Assay of DBtagged Proteins on Agarose/DNA Microplate

1. Prepare biotinylated substrate proteins (DBtag-PAK2-bls) by the cell-free system.
2. Mix the biotinylated proteins with Alexa488-STA (final 10 μg/ml).
3. Incubate for 30 min at 26°C.
4. Spot the mixture on the agarose/DNA-coated glass plate as described above (Subheading 3.3.).
5. Cover the microplate with caspase-3 solution.
6. Incubate for 30 min at 26°C.

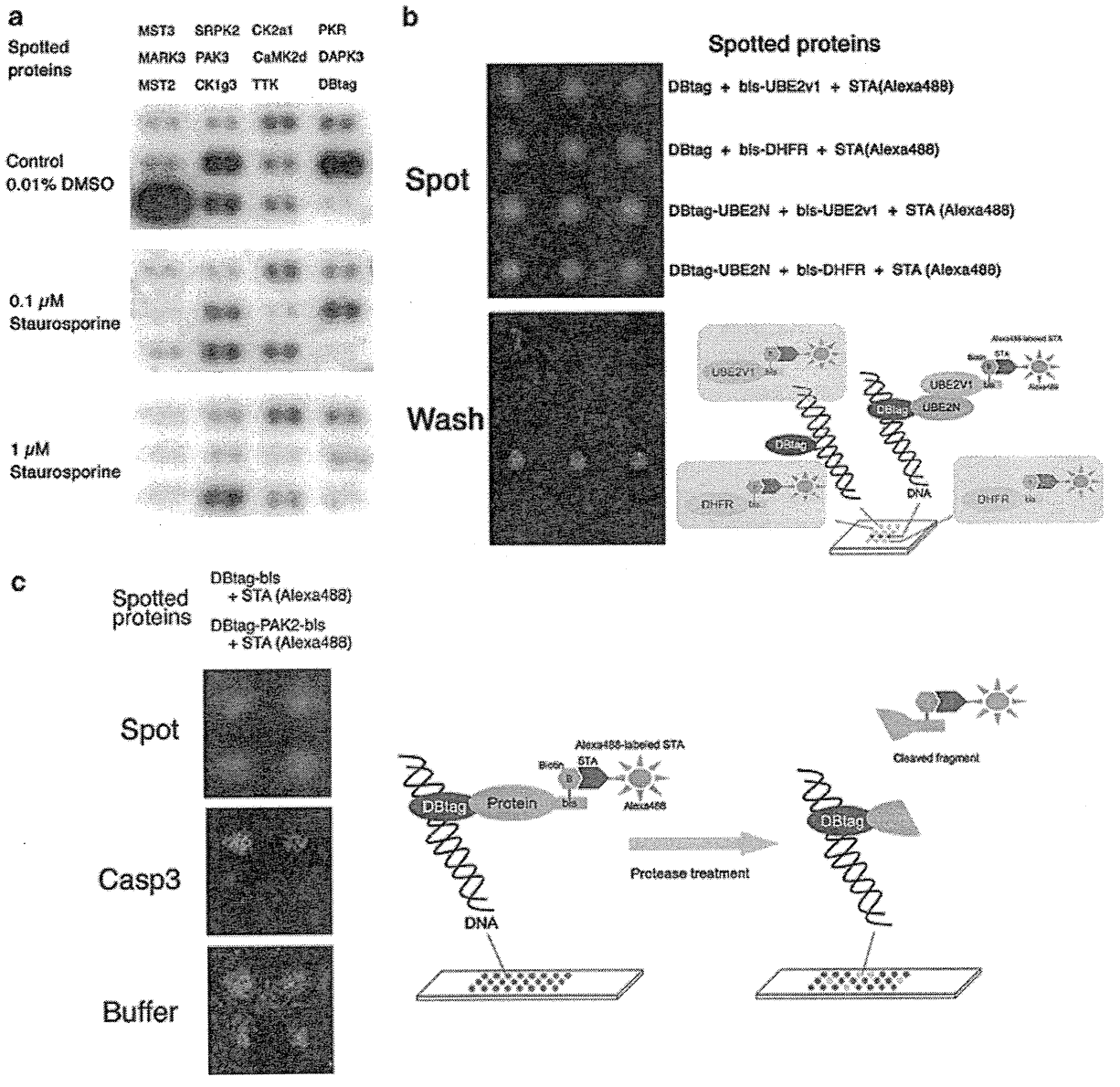

Fig. 7.2. (**a**) Detection and specific inhibition of the autophosphorylation activity of 11 human protein kinases on agarose/DNA microplate. The DBtagged human protein kinases were analyzed in duplicates. "DBtag" indicates the tag protein by itself (control). (**b**) Detection of a protein–protein interaction between UBE2N and UBE2v1 on the agarose/DNA microplate. Four samples (DBtag + biotin-labeled bls-UBE2v1 + STA(Alexa488), DBtag + biotin-labeled bls-DHFR + STA(Alexa488), DBtag-UBE2N + the bls-UBE2v1 + STA(Alexa488) and DBtag-UBE2N + the bls-DHFR + STA(Alexa488) from the top in "spot" panel] were spotted with three spots on the microplate. The first, second, and fourth samples lost the fluorescence after washing ("wash" panel). The third sample showed the fluorescence in "wash" panel, indicating a heterodimer as a protein–protein interaction between UBE2N and UBE2v1 proteins. An image from this result was shown in the *right panel*. (**c**) Two proteins including PAK2 (*lower spots* in each panel: DBtag-PAK2-bls labeled with Alexa488-STA) lost the fluorescence after the caspase 3 (casp3) treatment ("Casp3" panel). DBtag-bls proteins (*upper spots* in each panel: DBtag-bls labeled with Alexa488-STA) and buffer without the casp3 ("buffer" panel) showed fluorescence because they were not recognized by the casp3. *Right panel* indicates the schematic that the fluorescence-labeled region is released by the protease cleavage, and as a result, the fluorescence was lost upon washing.

7. Soak the microplate in 1× PBS buffer for 10 min (see Note 6).
8. Analyze the microplate by Typhoon 9400 imaging system.

4. Notes

1. Exonuclease I degrades extra primers after the PCR reaction. We often found primer contaminant in samples after Purification kit. The exonuclease I is very convenient to remove the extra primers because it is inactivated by simple heat treatment.
2. If DNA template is of low production, increase of primer concentration could provide higher production. In our case, the concentration increases to 100 nM from 10 nM as final concentration.
3. The agarose/slide-coated glass should be used within 1 day.
4. During spotting process, humidity inside the spotter should be kept. MultiSPRinter™ spotter can control high-humidity condition.
5. During making of the microplate and the assay, the microplate should be kept in a Tupperware box containing wet papers to prevent it from drying. Dried microplate could not be used for the functional analysis of proteins.
6. If soaking time is too long, assay sensitivity is decreased.

Acknowledgements

We greatly thank Satoko Matsunaga, Yuko Matsubara, Yoshiko Kodani, Yoshinori Tanaka, and two researchers (Mihoro Saeki and Dr. Ryo Morishita) working in CellFree Sciences Co., Ltd for their expert technical assistance. This work was partially supported by the Special Coordination Funds for Promoting Science and Technology by the Ministry of Education, Culture, Sports, Science and Technology, Japan.

References

1. Qin, S., Qiu, W., Ehrlich, J.R., Ferdinand, A.S., Richie, J.P., O'Leary M.P., Lee, M.L. and Liu, B.C. (2006) Development of a "reverse capture" autoantibody microarray for studies of antigen-autoantibody profiling. *Proteomics* **6**, 3199–3209.
2. Sheridan, C. (2005) Protein chip companies turn to biomarkers. *Nat. Biotechnol.* **23**, 3–4.
3. Zhu, H. and Snyder, M. (2003) Protein chip technology. *Curr. Opin. Chem. Biol.* **7**, 55–63.
4. Sawasaki, T., Ogasawara, T., Morishita, R. and Endo, Y. (2002) A cell-free protein

synthesis system for high-throughput proteomics. *Proc. Natl. Acad. Sci. USA.* **99,** 14652–14657.

5. Endo, Y. and Sawasaki, T. (2006) Cell-free expression systems for eukaryotic protein production. *Curr. Opin. Biotechnol.* **17,** 373–380.
6. Sawasaki, T., Gouda, M.D., Kawasaki, T., Tsuboi, T., Tozawa, Y., Takai, K. and Endo, Y. (2005) The wheat germ cell-free expression system: methods for high-throughput materialization of genetic information. *Methods Mol. Biol.* **310,** 131–144.
7. Sawasaki, T., Kamura, N., Matsunaga, S., Saeki, M., Tsuchimochi, M., Morishita, R. and Endo, Y. (2008) Arabidopsis HY5 protein functions as a DNA-binding tag for purification and functional immobilization of proteins on agarose/DNA microplate. *FEBS Lett.* **582,** 221–228.
8. Oyama, T., Shimura, Y. and Okada, K. (1997) The Arabidopsis HY5 gene encodes a bZIP protein that regulates stimulus-induced development of root and hypocotyl. *Genes Dev.* **11,** 2983–2995.
9. Kamura, N., Sawasaki, T., Kasahara, Y., Takai, K. and Endo, Y. (2005) Selection of 5′-untranslated sequences that enhance initiation of translation in a cell-free protein synthesis system from wheat embryos. *Bioorg. Med. Chem. Lett.* **15,** 5402–5406.
10. Sawasaki, T., Hasegawa, Y., Tsuchimochi, M., Kamura, N., Ogasawara, T. and Endo, Y (2002) A bilayer cell-free protein synthesis system for high-throughput screening of gene products. *FEBS Lett.* **514,** 102–105.

Development of the malaria parasite in the skin of the mammalian host

Pascale Gueirard[a], Joana Tavares[a], Sabine Thiberge[a], Florence Bernex[b], Tomoko Ishino[a,1], Genevieve Milon[c], Blandine Franke-Fayard[d], Chris J. Janse[d], Robert Ménard[a,2], and Rogerio Amino[a]

[a]Unité de Biologie et Génétique du Paludisme, Institut Pasteur, 75724 Paris Cedex 15, France; [b]Institut National de la Recherche Agronomique, UMR955 Génétique Fonctionnelle et Médicale and Unité d'Anatomie Pathologique, Ecole Nationale Vétérinaire d'Alfort, F-94700 Maisons-Alfort, France; [c]Unité d'Immunophysiologie et Parasitisme Intracellulaire, Institut Pasteur, 75724 Paris Cedex 15, France; and [d]Department of Parasitology, Centre of Infectious Diseases, Leiden University Medical Centre, 2300 RC, Leiden, The Netherlands

Edited* by Louis H. Miller, National Institutes of Health, Rockville, MD, and approved September 8, 2010 (received for review July 5, 2010)

The first step of *Plasmodium* development in vertebrates is the transformation of the sporozoite, the parasite stage injected by the mosquito in the skin, into merozoites, the stage that invades erythrocytes and initiates the disease. The current view is that, in mammals, this stage conversion occurs only inside hepatocytes. Here, we document the transformation of sporozoites of rodent-infecting *Plasmodium* into merozoites in the skin of mice. After mosquito bite, ~50% of the parasites remain in the skin, and at 24 h ~10% are developing in the epidermis and the dermis, as well as in the immunoprivileged hair follicles where they can survive for weeks. The parasite developmental pathway in skin cells, although frequently abortive, leads to the generation of merozoites that are infective to erythrocytes and are released via merosomes, as typically observed in the liver. Therefore, during malaria in rodents, the skin is not just the route to the liver but is also the final destination for many inoculated parasites, where they can differentiate into merozoites and possibly persist.

intravital imaging | *Plasmodium* | schizogony

Malarial infection starts with the inoculation of *Plasmodium* sporozoites by mosquitoes probing the vertebrate skin for blood. The highly motile sporozoites eventually invade host target cells where they differentiate and divide into numerous merozoites, the parasite form that invades erythrocytes and initiates the pathogenic phase of malarial infection. The host cell type in which sporozoites transform into merozoites, however, differs between *Plasmodium* species. In species that infect birds, sporozoites differentiate inside macrophages primarily in the skin but also in the spleen, liver, and bone marrow (1). In species that infect mammals, sporozoites are known to differentiate only inside hepatocytes in the liver (2–4).

The first demonstration that sporozoites of mammal-infecting *Plasmodium* species develop inside hepatocytes was made in 1948 after i.v. inoculation of sporozoites of *P. cynomologi* into rhesus monkeys (2). In addition to reporting fully mature parasites inside hepatocytes, the authors also documented the persistence of immature and dormant forms of the parasite in the liver several months after the initial inoculation, which they proposed to be the cause of relapses (5), and were later called hypnozoites (6). Subsequent work indicated that sporozoites of species that infect humans (7) also undergo complete development inside hepatocytes.

Since these early studies, *P. berghei* and the related *P. yoelii* species, which infect rodents, have been used as practical and safe models for studying the pre-erythrocytic phase of malaria. These parasites were shown to differentiate in the liver of laboratory rodents (8), and the *P. berghei*/rodent system was used to demonstrate that the majority of sporozoites were inoculated by mosquitoes in the skin rather than directly into the blood circulation (9), as traditionally assumed. More recently, the generation of fluorescent *P. berghei* parasites, along with the development of intravital imaging approaches applicable to rodents, have allowed rapid progress in our understanding of the fate of *Plasmodium* sporozoites in the mammalian host.

Intravital imaging of *P. berghei* sporozoites confirmed that sporozoites were injected in the skin of the mouse, where they display vigorous motility (10). Quantitative analysis revealed that more than half of the *P. berghei* sporozoites inoculated by mosquitoes in the mouse ear skin were still present at the bite site after 1 h (11), and ~40% stayed as long as 6 h (12), when sporozoites are no longer actively motile. Of the sporozoites that left the mosquito bite site, ~70% were found to take the blood route and ~30% the lymphatic route (11). The latter terminate their journey in the first draining lymph node, where most die in a few hours, though a few develop, at least partially, in association with podoplanin-expressing cells (11). A similar tripartite fate of sporozoites staying in the skin, leaving the skin via the blood or via the lymph, was later also described for *P. yoelii* using quantitative PCR analysis (13).

In this work, we analyze the fate of sporozoites of rodent-infecting *Plasmodium* species in the skin of mice.

Results and Discussion

***P. berghei* Develops Inside Skin Cells in the Mouse.** We first analyzed the fate of the *P. berghei* sporozoites that remain in the skin of the host. *Anopheles stephensi* mosquitoes were allowed to transmit WT green fluorescent sporozoites (14) into the ear of SKH1 *hairless* mice (15), which display little autofluorescence in the skin, and parasites were imaged daily using spinning-disk confocal microscopy (16). Typically, inside hepatocytes, parasites round up and increase their size to become spherical exoerythrocytic forms (EEF) of ~40-μm average diameter, undergo schizogony, and produce thousands of uninucleate merozoites in ~50–70 h (4). Approximately 11% of the elongated sporozoites detected in the skin soon after the bite were still observed after 24 h (day 1, D1) as brightly fluorescent, round parasites (Fig. 1*A* and *B*). The average size and fluorescence intensity of the EEF steadily increased with time (Fig. 1*A* and *C*). However, the maximal diameter of skin EEF, typically reached at D3–D4, remained 2–3 times smaller than the maximal diameter of liver EEF, reached at D2 (Fig. 1 *A* and *C*). When parasite survival was assessed after intradermal injection of ~5,000 sporozoites into the ear skin, only ~1% and 0.2% were found to brightly fluoresce at D1 and D4, respectively (Fig. 1 *D* and *C*). Despite the ~10-fold decrease in the percentage of parasites

Author contributions: P.G., J.T., S.T., T.I., G.M., R.M., and R.A. designed research; P.G., J.T., S.T., T.I., B.F.-F., C.J.J., and R.A. performed research; F.B., B.F.-F., and C.J.J. contributed new reagents/analytic tools; P.G., J.T., S.T., F.B., T.I., B.F.-F., C.J.J., R.M., and R.A. analyzed data; and R.M. and R.A. wrote the paper.

The authors declare no conflict of interest.

*This Direct Submission article had a prearranged editor.

[1]Present address: Department of Molecular Parasitology, Ehime University Graduate School of Medicine, Shitsukawa, Toon, Ehime 7910-0295, Japan.

[2]To whom correspondence should be addressed. E-mail: rmenard@pasteur.fr.

This article contains supporting information online at www.pnas.org/lookup/suppl/doi:10.1073/pnas.1009346107/-/DCSupplemental.

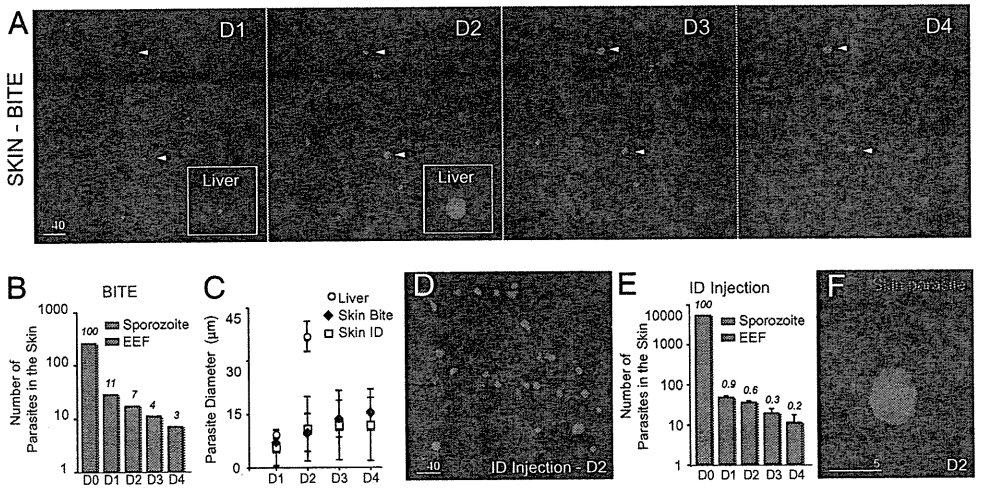

Fig. 1. *P. berghei* differentiation in the ear skin of a *hairless* mouse. (*A*) Parasites (in green) imaged for 4 d (autofluorescence in red) after sporozoite inoculation by the bite of a single mosquito. Images are maximal Z-projections of 13–21 contiguous pictures separated by 5 µm. Red arrowheads, fluorescent parasites fading over time; white arrowheads, brightly fluorescent parasites until day 4 (D4). The lower-right inset shows a liver stage at the same scale at D1 and D2. (Scale bar, 40 µm.) (*B*) Cumulative numbers of developing parasites in six different bite sites from two independent experiments. Orange bar (D0), number of sporozoites detected after the bite ($n = 258$); green bars, number of brightly fluorescent EEF; numbers above the bars, percentages of developing parasites versus sporozoites imaged at D0. (*C*) Parasite diameter (average ± SD), estimated by the EEF maximum projection area, in the liver (circles) and in the skin (diamond, after bite; square, after injection). (*D*) Parasites (in green) at D2 after microinjection of 5,200 sporozoites. The image is a maximal Z-projection of 35 pictures covering 70 µm in depth. (Scale bar, 40 µm.) (*E*) Numbers of developing parasites after intradermal injection. Orange bar (D0), no. of injected sporozoites (5,200); green bars, numbers of brightly fluorescent EEF (average ± SD), in four injection sites; numbers above the bars, percentages of developing parasites vs. sporozoites injected at D0. Similar results were obtained after injection of larger number of sporozoites (75,000–300,000 parasites). (*F*) Green fluorescent EEF surrounded by a parasitophorous vacuole stained with anti-UIS4 polyclonal antibody (in red) at D2. (Scale bar, 5 µm.)

present at D1 after needle injection compared with mosquito delivery, the fate of surviving parasites was similar in the two cases, as judged by the proportion (Fig. 1 *B* and *E*) and the average size (Fig. 1*C*) of fluorescent EEF.

We then asked whether parasite maturation in the skin occurred within host cells. In hepatocytes, parasites develop inside a parasitophorous vacuole (PV) formed upon sporozoite entry into the host cell (17). The sporozoite transmembrane protein UIS4 inserts into the PV membrane and is essential for liver-stage development (18). Staining of skin cryosections with anti-UIS4 antibodies (Fig. 1*F*) showed that 53% and 65% of the green fluorescent EEF were delineated by a clear red UIS4 signal at D1 and D2, respectively.

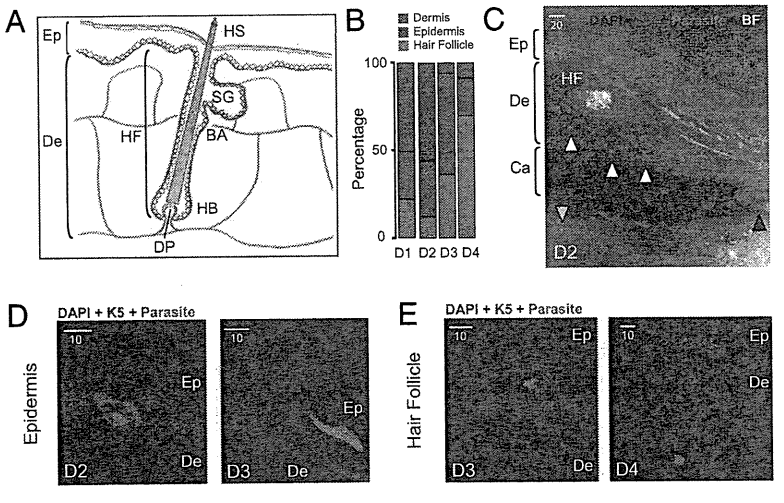

Fig. 2. Localization of *P. berghei* skin EEF. (*A*) Schematic view of the epidermis, dermis, and hair follicle of the mammalian skin. Drawn are the keratin5-positive keratinocytes (in red) that rest on the basement membrane separating the dermis from the epidermis and line the invagination of the HF; the Blimp1-positive cells (in green) associated with the superficial layer of the epidermis and the HF; and the vascularization in the dermis (red lines). Ep, epidermis; De, dermis; HF, hair follicle; HS, hair shaft; SG, sebaceous gland; BA, bulge area; HB, hair bulb; DP, dermal papilla. (*B*) Percentage of dermal (blue), epidermal (red), and hair follicle-associated (green) parasites in the mouse ear estimated by immunofluorescence microscopy at various days after intradermal injection of sporozoites. Number of analyzed EEF for each time point: 33–63. (*C*) Confocal image showing EEF (in green) in the deep dermis (white arrowheads), the epidermis (yellow arrowhead), and the cartilage (red arrowhead). Abbreviations are as in *A*; Ca, cartilage. (Scale bar, 20 µm.) (*D*) Confocal images of epidermal EEF (in green), associated with keratin5-positive keratinocytes of the basal layer of the epidermis (*Left*) or with keratin5-negative keratinocytes of the superficial layers of the epidermis (*Right*). Abbreviations are as in *A*. (Scale bar, 10 µm.) (*E*) Confocal images of hair follicle-associated EEF. EEF (in green) are located in the upper portion of the HF, in keratin5-positive or keratin5-negative cells, often near the sebaceous glands. Abbreviations are as in *A*. (Scale bar, 10 µm.)

We also analyzed the development in the mouse skin of sporozoites lacking the P36p protein. P36p is important for the formation and/or maintenance of the PV membrane, and a *P. berghei P36p* knockout clone generates ~5–10% of the EEF produced by WT sporozoites inside hepatocytes (19, 20). We constructed the *P. berghei* clone P36p-G bearing both the *P36p*- null mutation and a GFP-expression cassette (Fig. S1), and sporozoites of the clone were coinjected with red-fluorescent WT sporozoites of the L733 clone (21) into the skin of mice. Approximately 10-fold fewer green P36p-G than red WT EEF were observed at D1 at the injection site (Fig. S1). Together, these data suggested that most WT *P. berghei* parasites surviving in the mouse skin were developing intracellularly inside a PV.

***P. berghei* Develops in the Epidermis and Dermis and in Association with Hair Follicles.** We next localized the EEF in the skin using an immunohistological approach (see Fig. 2*A* for a schematic representation of the mammalian skin). *P. berghei* sporozoites (2×10^5) were injected into the ear skin of *hairless* mice, and at various days postinoculation ~10-μm cryosections of fixed ear tissues were labeled with DAPI and immunostained using antibody K5, which recognizes keratin5 in keratinocytes of the basal layer of the epidermis (22). EEF were present in multiple sites in the skin. (*i*) At D1 and D2, ~50% of the EEF were located in the dermis (Fig. 2 *B* and *C* and Fig. S2*A*). Dermal EEF behaved similarly to liver EEF, with a sharp decrease between D2 and D3, and only represented ~7% of the skin EEF at D3 and D4 (Fig. 2*B*). (*ii*) EEF were also found in the epidermis. At D1 and D2, epidermal EEF were associated mostly with keratin5-positive keratinocytes lying on the basement membrane, whereas at D3 and D4 they were mostly in keratin5-negative cells in the superficial layers of the epidermis (Fig. 2*D* and Fig. S2*B*). The number of epidermal EEF did not significantly change up to D3, and only slightly decreased at D4 (Fig. 3*A*). (*iii*) More surprisingly, EEF were found in close association with hair follicles, appearing as keratin5-positive keratinocyte-bound tubular invaginations of the epidermis (Fig. 2*E* and Fig. S2*C*). In *hairless* mice, EEF associated with the autofluorescent (and rudimentary) hair follicles were frequently located close to the sebaceous glands (Fig. 2*E* and Fig. S2*C*). Their numbers remained stable up to D4 (Fig. 3*A*), representing 70% of the skin EEF at D4 (Fig. 2*B*), and parasites were still detected in hair follicles after more than 2 wk postinoculation (Fig. 3*B*).

Parasite association with hair follicles was also imaged in a Blimp1-GFP mouse (23). In this mouse, a group of cells expressing the transcriptional repressor B lymphocyte-induced maturation protein 1 (Blimp1) and residing near the bud site of the sebaceous glands, which act as sebocyte progenitor cells, are green fluorescent (24). After injection of red fluorescent WT sporozoites into the ear of a Blimp1-GFP mouse, red fluorescent EEF were found associated with the green fluorescent area of hair follicles (Fig. 3*C*, skin). As in the hairless mice, hair follicle-associated EEF were observed persisting for several days, in the vicinity of the GFP-fluorescent zone of the sebaceous glands (Fig. 3*C*, hair follicle). It is still unclear, however, whether these parasites were simply growing slowly in the skin or might include true dormant (growth-arrested) forms.

***P. berghei* Developing in the Mouse Skin Generates Merozoites.** We next imaged parasite growth in the skin using bioluminescence. For this, we used sporozoites of the transgenic *P. berghei* clone 676cl1 (Pb*GFP-LUC*$_{SCH}$) expressing a GFP-luciferase fusion gene via the *EEF1α* promoter (25), which constitutively produces the fusion protein throughout the parasite life cycle. Sporozoites (2×10^4) were inoculated in the ear skin of mice and luciferin injected immediately before real-time whole-body imaging of mice using the IVIS system (26). Bioluminescent signals were detected only in the ear and the liver at D2 (Fig. S3). The main signal was detected in the liver, peaking at D2, and the signal in the ear skin peaked at D3.

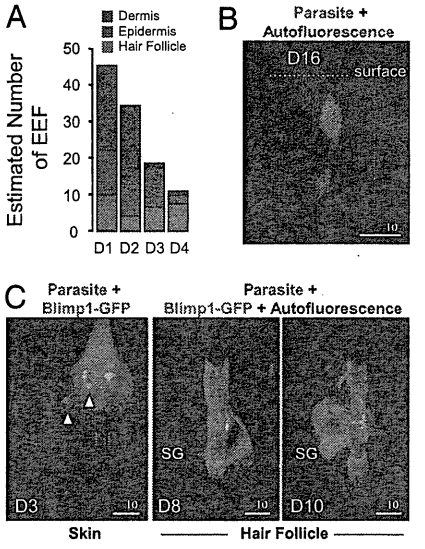

Fig. 3. *P. berghei* association with hair follicles. (*A*) Numbers of dermal, epidermal, and hair follicle-associated EEF after intradermal injection of sporozoites, obtained by multiplying the numbers of skin EEF counted by intravital microscopy (Fig. 1*E*) by the percentages of dermal, epidermal, and hair follicle-associated parasites counted by histology (Fig. 2*B*). (*B*) Intravital confocal image showing EEF surviving inside a hair follicle in the ear of a *hairless* mouse at D16 after microinjection of sporozoites. The images are a lateral view of a 3D reconstruction of the skin. Parasites are in green and the hair follicle autofluoresces in red. (Scale bar, 10 μm.) (*C*) Intravital confocal images showing red fluorescent EEF in the ear skin of a Blimp1-GFP mouse. (*Left*) D3: Z-projection of 70 slices covering 35 μm showing red fluorescent EEF inside a hair follicle (white arrowheads). (*Center*) D8 and (*Right*) D10: red EEF in a hair follicle in close association with Blimp1-GFP-positive cells. (Scale bars, 10 μm.)

Quantification of the intensity of bioluminescence signals using the Living Image software showed that the signal in the ear skin increased ~threefold between D1 and D2, and ~2.5-fold between D2 and D3 (Fig. 4*A*). This suggested that, like liver parasites, skin parasites could actively grow.

To investigate schizogony in skin parasites, we examined individual skin EEF at D3 and D4, when most had reached their maximal size, by confocal microscopy. In *hairless* mice, fluorescent parasites were seen undergoing nuclear divisions (Fig. S4) and generating individual merozoite-like progeny (Fig. 4*B*). Further, infected cells in the skin were frequently observed giving rise to cell extensions reminiscent of the merosomes that extrude from infected hepatocytes (Fig. S5*A*). Hepatocyte-derived merosomes contain tens to thousands of merozoites wrapped in the host cell membrane, bud off, and detach from the infected cell to reach the blood in the liver sinusoids (27). Brightly fluorescent merosome-like extensions were also observed detaching from infected cells (Fig. 4*C*) and moving in the skin (Fig. 4*C* and Fig. S5*B*).

To test whether the fluorescent progeny seen inside skin cells were indeed merozoites, we tested their capacity to invade and multiply in mouse erythrocytes. One day after injection of green fluorescent sporozoites into the skin of mice ($1.0–2.5 \times 10^5$ sporozoites per ear in 2–4 animals), i.e., before the first merozoites are formed in the liver, the skin tissue at the injection site was dissected and treated with collagenase and trypsin to obtain a single cell suspension. Infected fluorescent cells were sorted by FACS (Fig. 5*A*) and incubated for several days at 37 °C in vitro in DMEM 10% FCS. Examination of the sorted cells confirmed the diversity of skin cell types that were infected in situ (Fig. 5*B*), and after 4 d (1 d in the skin and 3 d in vitro), merozoites were detected inside sorted cells (Fig. 5*C*). At D4, cells were scratched and the host cell/

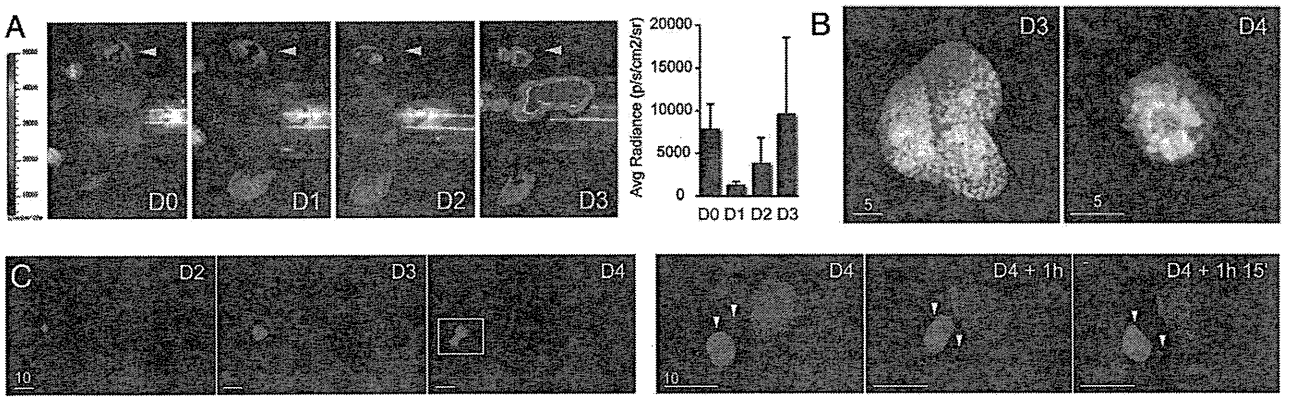

Fig. 4. *P. berghei* complete development inside skin cells. (*A*) Parasite development in the skin measured by bioluminescence. The 2 × 10^4 GFP::LUC sporozoites were microinjected in the ear of C57BL6 mice (yellow arrowhead) and recorded from D0 to D3 following injection of luciferin. The graph represents the difference between the average radiance of the inoculated ear and the contralateral ear at D0, 1, 2, and 3 (mean ± SD; $n = 3$). (*B*) Mature schizonts in the skin. Intravital imaging of merozoite-filled EEF in the ears of mice at D3 and D4. (Scale bars, 5 μm.) (*C*) Skin EEF release merosomes. (*Left*) Skin EEF growing and budding between D3 and D4 after mosquito bite. (*Right*) Time-lapse recording of the squared area depicted at D4 and shows the release and movement of fluorescent structures of various sizes. White arrowheads, merosomes; red arrowheads, merozoites. (Scale bars, 10 μm.)

parasite mixture injected i.v. into mice. In three independent experiments (Fig. 5*D*), mice became infected and parasitemia increased at a normal rate (~10-fold increase/24 h). This demonstrates that *P. berghei* development in skin cells can generate infective merozoites, and thus that the parasite developmental pathway in the skin indeed reproduced that in the liver.

In Situ Infectivity of *P. berghei* Merozoites Generated in Skin Cells. To test whether merozoites generated in skin cells (skin-derived merozoites) were capable of invading erythrocytes in situ and sufficient for generating a blood stage infection, transplantation experiments of infected skins onto naive mice were complicated by the different timings of maximal release of skin-derived merozoites (D2–D3 post-sporozoite inoculation) and of efficient vascularization of the skin graft. Strikingly, we observed that primaquine, a drug known to inhibit liver EEF development, had a much weaker effect on skin EEF development (Fig. S6*A*). After injection of luciferase-producing sporozoites in the ear of mice, treatment with 25 mg/kg primaquine at D0 and D1 abolished the bioluminescence signal in the liver without affecting that in the ear. However, this differential primaquine effect could not be exploited to show the in vivo infectivity of skin-derived merozoites. Indeed, the 25-mg/kg primaquine treatment did not completely prevent liver EEF maturation in all animals (5 of 52 primaquine-treated mice and surgically deprived of the infected ear at D1 became patent; see Fig. S7) and impaired skin EEF development between D2 and D3 (Fig. S6*A*), whereas 30 mg/kg primaquine significantly affected skin EEF development at earlier time points (Fig. S6*A*).

In any case, the skin-derived merozoites are clearly outnumbered by their liver-derived counterparts, and their contribution to the onset of blood stage infection would be minimal at best. After injection of luciferase-producing sporozoites in the skin of mice, the maximal intensity signal at the injection site, reached at D3, was found to be ~2% of the maximal intensity signal in the liver, reached at D2 (Fig. S6*B*). Not surprisingly, when sporozoites were injected in the ear of mice and the infected or controlateral ear was surgically removed at D1, no statistical difference was detected in the parasitemia of animals lacking or having skin EEF (Fig. S6*C*).

***P. yoelii* Generates Merozoites in the Mouse Skin.** Last, we studied the development of sporozoites of *Plasmodium yoelii*, another species that infects rodents, in the mouse skin. Like sporozoites of *P. falciparum*, the species most lethal to humans, *P. yoelii* sporozoites are known to invade only certain hepatocytic lines in vitro, in a CD81-dependent manner (28). Additionally, quantitative PCR analysis of mouse ear inoculated with *P. yoelii* sporozoites showed that the parasite DNA was still detected 42 h postinjection in the mouse skin (13). We analyzed the fate of *P. yoelii* sporozoites expressing GFP (29) or RedStar (Fig. S8) after intradermal injection in mice. At D1, ~0.2% and ~0.15% of the inoculated sporozoites transformed in the ear skin of *hairless* and Swiss mice, respectively (Fig. S9*A*). Despite the ~fivefold smaller

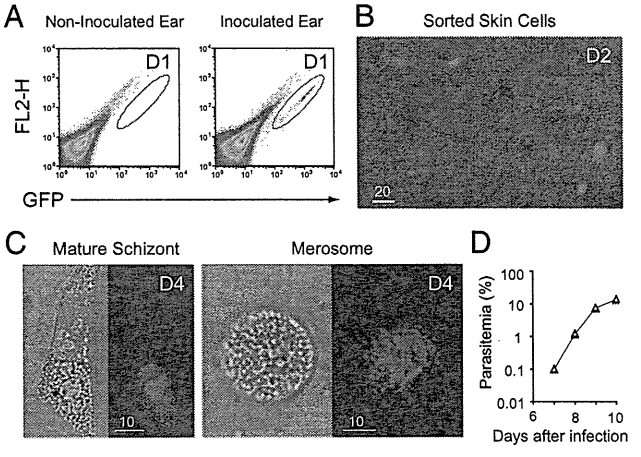

Fig. 5. Merozoite production by and in vivo infectivity of *P. berghei* skin EEF. (*A*) Sorting of infected skin cells. The 1.0–2.5 × 10^5 sporozoites were microinjected in the ear of C57BL6 mice. The pseudocolor plot shows the distribution of skin cells obtained from the ears of noninfected (*Left*) and infected mice (*Right*) 1 d postinfection. The green oval represents the gate used for sorting the infected skin cells, which were collected in 96-wells cell culture plate and kept at 37 °C, 5% CO_2 in DMEM 10% FCS. No events were detected using the noninfected ear. (*B*) Wide-field microscopy of sorted cells showing the variety of infected skin cell types (bright field and green) at D2—1 d in the skin and 1 d in vitro. (Scale bar, 20 μm.) (*C*) Generation of merozoites within skin cells. Presence of merozoites inside an adherent skin cell (*Left*) and in a floating merosome (*Right*). (Scale bar, 10 μm.) (*D*) A representative parasitemia curve following injection of merozoite-filled skin cells at D4—1 d in the skin and 3 d cultured in vitro. The number of events sorted at D1 in this experiment was 1,200 (~600 GFP^+ cells), resulting in approximately four mature schizonts after 3 d in culture. The parasitemia was accessed by FACS and blood smear.

number of *P. yoelii* parasites observed in the skin compared with *P. berghei* at D1, *P. yoelii* EEF, like *P. berghei* EEF, grew both in the epidermis and the dermis of mice (Fig. S9*B*). *P. yoelii* merozoites were detected from D2 onward (Fig. S9*C*) and were seen moving across the skin (Fig. S9*D*), indicating that *P. yoelii* EEF completed their development in the skin of mice.

Conclusions

This study shows that the *P. berghei* and *P. yoelii* rodent-infecting species can undergo complete exoerythrocytic schizogony not just inside hepatocytes but also inside skin cells. However, although the *P. berghei* infective merozoites released and moving in the skin in merosome-like extensions might occasionally invade erythrocytes in the mouse, and thus constitute a potential secondary reservoir of infective merozoites, skin-derived merozoites do not significantly contribute to erythrocyte infection in normal conditions. Whether other mammal-infecting *Plasmodium* species, particularly the human-infecting species, can also develop in the skin of the host remains to be addressed.

The data also suggest that parasites might persist in association with hair follicles, which constitute an immunoprivileged site of the mammalian body characterized by the virtual absence of major histocompatibility complex (MHC) class I expression and a strongly immunosuppressive environment (30). This raises the hypothesis that parasites might become quiescent when associated with hair follicles and act as a source of infection relapses, as proposed for the hypnozoites of *P. vivax* in the liver (31).

Perhaps the most important implication of this work is immunological. Whereas previous data (11, 12) showed that in the mouse ear model about half of the *P. berghei* sporozoites inoculated by mosquitoes stayed at the bite site, the present data indicate that ~10% of the injected sporozoites are developing at D1 in the skin. This implies that the lymph node that drains the injection site will receive parasite antigens not just from sporozoites (sporozoites actively reaching the lymph node or dead sporozoites left in the skin) but also from differentiating parasites (skin EEF aborting at various stages of their development). Overall, in the *P. berghei*/ear skin model system, the draining lymph node receives up to 70% of the parasite antigens inoculated by mosquito bite. The tolerogenic or protective properties of the various kinds of skin-derived parasite antigens will have to be assessed, in natural as well as immunizing conditions. This would be particularly important in the case of live attenuated (irradiated or genetically modified) sporozoites, which have been known for many years to act as powerful vaccines in animal models (32) and will soon undergo human trials (33–35), because in humans they can only be inoculated in the skin.

Materials and Methods

Parasites, Mice, and Mosquitoes. We used the *P. berghei* ANKA clone expressing GFP under the control of the *hsp70* promoter (14). The *P. yoelii* GFP-expressing parasite clone was obtained from the MR4 repository (ATCC no. MRA-817; 17XNL PYGFP). The red fluorescent *P. berghei* line (line 733) contains the RedStar-expressing cassette integrated at the *230p* genomic locus. The red fluorescent *P. yoelii* clone contains the RedStar cassette integrated at the *d-ssu-rrna* locus. We used the *P. berghei* clone 676cl1 (Pb*GFP-LUC*$_{SCH}$) expressing a GFP-luciferase fusion gene via the *EEF1α* promoter (25). C57BL/6, Swiss and *hairless* SKH1 mice were purchased from Charles River Laboratories. All experiments were approved by the committee of Institut Pasteur and were performed in accordance with the applicable guidelines and regulations. *A. stephensi* (Sda500 strain) mosquitoes were reared using standard procedures (16). For intradermal injection of sporozoites into rodents, salivary gland sporozoites were dissected out and a small volume (0.2–10 μL) containing 5×10^3 to 3×10^5sporozoites was deposited in the dermis of the ear by using a 35- to 36-gauge needle with a NanoFil syringe (World Precision Instruments).

Intravital Imaging and Immunolabelings. Intravital imaging was performed as described (16). For immunolabelings, ears were excised, fixed with 4% paraformaldehyde/PBS for 2 h, and dehydrated in 10% and 30% sucrose/PBS before embedding in OCT. Ten-micrometer sections were cut on a CM3050S cryostat (Leica) and adhered to Superfrost Plus Slides (VWR). Sections were permeabilized and blocked in PBS containing 0.1% Triton X-100 (Sigma) and 5% FCS, followed by staining with anti-keratin5 polyclonal primary antibody (Covance) or anti-UIS4 polyclonal primary antibody, AlexaFluor 546 conjugate (Molecular Probes), and DAPI (Molecular Probes). Stained slides were mounted with Prolong Gold (Invitrogen), and 3D image stacks were acquired on a SP5 confocal microscope (Leica). Images are displayed as 2D maximum-intensity projections.

ACKNOWLEDGMENTS. We thank Stéphane Vincent (Institut Pasteur) and Mitinori Saitou (Riken Center for Developmental Biology) for the kind gift of Blimp1-GFP mice. We thank Spencer Shorte, Marie Nguyen-de Bernon, and Marie-Anne Nicola and the Imagopole team (Institut Pasteur) for help with microscopy, cytometry, and bioluminescence; Catherine Bourgouin, Isabelle Thiéry and the other members of the CEPIA platform (Institut Pasteur) for rearing mosquitoes; Masao Yuda (Mie University) for the gift of anti-HSP70 antibodies; Stephan Kappe (Seattle Biomedical Research Institute) for the gift of anti-UIS4 antibodies; and Jean-Jacques Panthier and Geneviève Aubin-Houzelstein (Institut Pasteur) for helpful discussions. We acknowledge funding from Fundação para a Ciência e Tecnologia Grant SFRH/BPD/48340/2008 (to J.T.) and Institut Pasteur, Natixis, the BioMalPar European Network of Excellence, the Agence Nationale pour la Recherche, and the Howard Hughes Medical Institute (to R.M.).

1. Huff CG (1947) Life cycle of malarial parasites. *Annu Rev Microbiol* 1:43–60.
2. Shortt HE, Garnham PC (1948) Pre-erythrocytic stage in mammalian malaria parasites. *Nature* 161:126.
3. Vanderberg JP (1981) *Plasmodium berghei* exoerythrocytic forms develop only in the liver. *Trans R Soc Trop Med Hyg* 75:904–905.
4. Meis JF, Verhave JP (1988) Exoerythrocytic development of malarial parasites. *Adv Parasitol* 27:1–61.
5. Shortt HE, Garnham PC (1948) Demonstration of a persisting exo-erythrocytic cycle in *Plasmodium cynomolgi* and its bearing on the production of relapses. *BMJ* 1: 1225–1228.
6. Krotoski WA, et al. (1982) Demonstration of hypnozoites in sporozoite-transmitted *Plasmodium vivax* infection. *Am J Trop Med Hyg* 31:1291–1293.
7. Shortt HE, Fairley NH, Covell G, Shute PG, Garnham PC (1951) The pre-erythrocytic stage of *Plasmodium falciparum*. *Trans R Soc Trop Med Hyg* 44:405–419.
8. Yoeli M, Vanderberg JP, Upmanis RS, Most H (1965) Primary tissue phase of *Plasmodium berghei* in different experimental hosts. *Nature* 208:903.
9. Sidjanski S, Vanderberg JP (1997) Delayed migration of *Plasmodium* sporozoites from the mosquito bite site to the blood. *Am J Trop Med Hyg* 57:426–429.
10. Vanderberg JP, Frevert U (2004) Intravital microscopy demonstrating antibody-mediated immobilisation of *Plasmodium berghei* sporozoites injected into skin by mosquitoes. *Int J Parasitol* 34:991–996.
11. Amino R, et al. (2006) Quantitative imaging of *Plasmodium* transmission from mosquito to mammal. *Nat Med* 12:220–224.
12. Kebaier C, Voza T, Vanderberg JP (2009) Kinetics of mosquito-injected *Plasmodium* sporozoites in mice: Fewer sporozoites are injected into sporozoite-immunized mice. *PLoS Pathog* 5:e1000399.
13. Yamauchi LM, Coppi A, Snounou G, Sinnis P (2007) *Plasmodium* sporozoites trickle out of the injection site. *Cell Microbiol* 9:1215–1222.
14. Ishino T, Orito Y, Chinzei Y, Yuda M (2006) A calcium-dependent protein kinase regulates *Plasmodium* ookinete access to the midgut epithelial cell. *Mol Microbiol* 59: 1175–1184.
15. Panteleyev AA, et al. (1998) Towards defining the pathogenesis of the hairless phenotype. *J Invest Dermatol* 110:902–907.
16. Amino R, et al. (2007) Imaging malaria sporozoites in the dermis of the mammalian host. *Nat Protoc* 2:1705–1712.
17. Baldacci P, Ménard R (2004) The elusive malaria sporozoite in the mammalian host. *Mol Microbiol* 54:298–306.
18. Mueller AK, et al. (2005) *Plasmodium* liver stage developmental arrest by depletion of a protein at the parasite-host interface. *Proc Natl Acad Sci USA* 102:3022–3027.
19. Ishino T, Chinzei Y, Yuda M (2005) Two proteins with 6-cys motifs are required for malarial parasites to commit to infection of the hepatocyte. *Mol Microbiol* 58: 1264–1275.
20. van Dijk MR, et al. (2005) Genetically attenuated, P36p-deficient malarial sporozoites induce protective immunity and apoptosis of infected liver cells. *Proc Natl Acad Sci USA* 102:12194–12199.
21. Sturm A, et al. (2009) Alteration of the parasite plasma membrane and the parasitophorous vacuole membrane during exo-erythrocytic development of malaria parasites. *Protist* 160:51–63.
22. Dai X, Segre JA (2004) Transcriptional control of epidermal specification and differentiation. *Curr Opin Genet Dev* 14:485–491.
23. Ohinata Y, et al. (2005) Blimp1 is a critical determinant of the germ cell lineage in mice. *Nature* 436:207–213.

24. Horsley V, et al. (2006) Blimp1 defines a progenitor population that governs cellular input to the sebaceous gland. *Cell* 126:597–609.
25. Franke-Fayard B, et al. (2008) Simple and sensitive antimalarial drug screening in vitro and in vivo using transgenic luciferase expressing *Plasmodium berghei* parasites. *Int J Parasitol* 38:1651–1662.
26. Franke-Fayard B, Waters AP, Janse CJ (2006) Real-time in vivo imaging of transgenic bioluminescent blood stages of rodent malaria parasites in mice. *Nat Protoc* 1: 476–485.
27. Sturm A, et al. (2006) Manipulation of host hepatocytes by the malaria parasite for delivery into liver sinusoids. *Science* 313:1287–1290.
28. Silvie O, et al. (2003) Hepatocyte CD81 is required for *Plasmodium falciparum* and *Plasmodium yoelii* sporozoite infectivity. *Nat Med* 9:93–96.
29. Ono T, Tadakuma T, Rodriguez A (2007) *Plasmodium yoelii yoelii* 17XNL constitutively expressing GFP throughout the life cycle. *Exp Parasitol* 115:310–313.
30. Mellor AL, Munn DH (2006) Immune privilege: A recurrent theme in immunoregulation? *Immunol Rev* 213:5–11.
31. Cogswell FB (1992) The hypnozoite and relapse in primate malaria. *Clin Microbiol Rev* 5:26–35.
32. Mulligan HW, Russell PF, Mohan BN (1941) Active immunization of fowls against *Plasmodium gallinaceum* by injections of killed homologous sporozoites. *J Malaria Inst India* 4:25–34.
33. Luke TC, Hoffman SL (2003) Rationale and plans for developing a non-replicating, metabolically active, radiation-attenuated *Plasmodium falciparum* sporozoite vaccine. *J Exp Biol* 206:3803–3808.
34. Matuschewski K (2006) Vaccine development against malaria. *Curr Opin Immunol* 18: 449–457.
35. Mikolajczak SA, Aly AS, Kappe SH (2007) Preerythrocytic malaria vaccine development. *Curr Opin Infect Dis* 20:461–466.

Am. J. Trop. Med. Hyg., 84(2), 2011, pp. 292–297
doi:10.4269/ajtmh.2011.10-0432

Genetic Polymorphism of *Plasmodium vivax msp1p*, a Paralog of Merozoite Surface Protein 1, from Worldwide Isolates

Yue Wang,† Osamu Kaneko,† Jetsumon Sattabongkot, Jun-Hu Chen, Feng Lu, Jong-YilChai, Satoru Takeo, Takafumi Tsuboi, Francisco J. Ayala, Yong Chen, Chae Seung Lim, and Eun-Taek Han*

Department of Parasitology, Kangwon National University College of Medicine, Chuncheon, Gangwon-do, Republic of Korea; Institute of Parasitic Diseases, Zhejiang Academy of Medical Sciences, Hangzhou, People's Republic of China; Department of Protozoology, Institute of Tropical Medicine and the Global Center of Excellence Program, Nagasaki University, Nagasaki, Japan; Department of Entomology, Armed Forces Research Institute of Medical Sciences, Bangkok, Thailand; Jiangsu Institute of Parasitic Diseases, Wuxi, People's Republic of China; Department of Parasitology and Tropical Medicine, Seoul National University College of Medicine, Seoul, Republic of Korea; Cell-Free Science and Technology Research Center, Ehime University, Ehime, Japan; Department of Ecology and Evolutionary Biology, University of California, Irvine, California; Zhejiang Medical College and Zhejiang Academy of Medical Sciences, Hangzhou, People's Republic of China; Department of Laboratory Medicine, College of Medicine, Korea University, Seoul, Republic of Korea

Abstract. *Plasmodium vivax msp1p*, a paralog of the candidate vaccine antigen *P. vivax* merozoite surface protein 1, possesses a signal peptide at its N-terminus and two epidermal growth factor–like domains at its C-terminus with a glycosylphosphatidylinositol attachment site. The *msp1p* gene locus may have originated by a duplication of the *msp1* gene locus in a common ancestor of the analyzed *Plasmodium* species and lost from *P. yoelii*, *P. berghei*, and *P. falciparum* during their evolutionary history. Full-length sequences of the *msp1p* gene were generally highly conserved; they had a few amino acid substitutions, one highly polymorphic E/Q-rich region, and a single-to-triple hepta-peptide repeat motif. Twenty-one distinguishable allelic types (A1–A21) of the E/Q-rich region were identified from worldwide isolates. Among them, four types were detected in isolates from South Korea. The length polymorphism of the E/Q-rich region might be useful as a genetic marker for population structure studies in malaria-endemic areas.

INTRODUCTION

Among the species of malarial parasite that infect humans, *Plasmodium vivax* is the most globally prevalent and threatens almost 40% of the world's population, resulting in approximately 250 million clinical infections each year.[1] Although *P. vivax* malaria had been considered relatively benign, compared with that of *P. falciparum*, this view is now being challenged. Additionally, resistance to chloroquine is appearing in countries where malaria is endemic.[2] Thus, there are good reasons to pursue an effective *P. vivax* vaccine.[3] In this regard and in contrast to *P. falciparum*, research into *P. vivax* is limited, due in part to difficulties in culturing blood-stage parasites *in vitro*.[4] Nevertheless, several *P. vivax* vaccine candidates from different parasitic stages have been characterized.[5] Among them, various merozoite surface proteins (MSPs), apical membrane protein-1, duffy binding protein, Pvs25, Pvs28, circumsporozoite protein, and thrombospondin-related anonymous protein have been studied.[5]

Merozoite surface proteins have been characterized and are highly immunogenic in natural infection.[6–9] Among them, several major vaccine candidate antigens (including MSP1, MSP4, MSP5, MSP8, and MSP10) are either known or presumed glycosylphosphatidylinositol (GPI)–anchored membrane proteins. *Plasmodium vivax* MSP1 is the largest and most abundant protein on the *P. vivax* merozoite surface.[5,10] The gene that encodes this protein (*Pvmsp1*) is highly polymorphic and consists of a mosaic of conserved and variable blocks with numerous recombination sites distributed throughout the gene. However, the fragment that encodes the 19-kDa C-terminal epidermal growth factor (EGF)–like domain is relatively conserved.[11] This gene has been used as a polymorphic marker for investigations of the genetic structure of *P. vivax* populations and in molecular epidemiology.[12]

With the completion of *P. vivax* genome sequencing, GPI-anchored proteins of *P. vivax* have been predicted by comparison with validated *P. falciparum* GPI-anchored proteins.[13,14] *Plasmodium vivax msp1p* (*Pvmsp1p*), a novel paralog of the *Pvmsp1* gene, was found immediately upstream of *Pvmsp1*.[14] This gene is predicted to encode a 1,854-amino-acid protein (predicted molecular mass of 215 kDa) with an N-terminal signal sequence, C-terminal EGF-like domains, and a GPI-attachment motif (Figure 1).[14] The functions of this molecule remain unknown. Thus, we have analyzed available genomic data from PlasmoDB (http://www.plasmodb.org/) to search for distinctive pattern of diversity in *msp1p* and *msp1* genes among *Plasmodium* species. We have also assessed the nature and extent of polymorphisms in PvMSP1P from worldwide isolates and laboratory lines of *P. vivax*.

MATERIALS AND METHODS

Gene sequences. The following sequences of malarial parasites were used for the analyses: human *P. falciparum* PfMSP1 (CAA27070), PfMSP8 (PFE0120c), and PfMSP10 (PFF0995c), and *P. vivax* PvMSP1 (PVX_099980), PvMSP8 (PVX_097625), PvMSP10 (PVX_114145), and PvMSP1P (PVX_099975); rodent malaria *P. berghei* PbMSP1 (AAC28871), PbMSP8 (PBANKA_110220), and PbMSP10 (PBANKA_111960), *P. yoelii* PyMSP1 (PY05748), and *P. chabaudi* PchMSP1 (PCAS_083080); primate malaria *P. knowlesi* PkMSP1 (PKH_072850) and PkMSP1P (PKH_072840), *P. reichenowi* PrMSP1 (CAH10285), and *P. cynomolgi* PcyMSP1 (BAI82251); and avian malaria *P. gallinaceum* PgMSP1 (CAH10838). The *P. gallinaceum* sequence database (http://www.sanger.ac.uk/) was used to search for homologs of PvMSP1P and PvMSP10.

Blood samples and DNA preparation. Blood samples were collected, after informed consent had been obtained, from 81

*Address correspondence to Eun-Taek Han, Department of Parasitology, Kangwon National University College of Medicine, Hyoja2-dong, Chuncheon, Gangwon-do 200-701, Republic of Korea. E-mail: ethan@kangwon.ac.kr
†These authors contributed equally to this article.

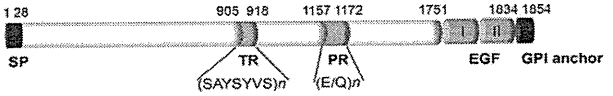

FIGURE 1. Schematic diagram of the *Plasmodium vivax* merozoite surface protein 1 paralog. A putative signal peptide (SP), the epidermal growth factor (EGF)–like domains, and the glycosylphosphatidylinositol (GPI)–anchor attachment site are indicated. TR = tandem repeat region of hepta-peptide; PR = polymorphic E/Q rich region. White color indicates region conserved among strains.

symptomatic patients diagnosed by microscopic examination with *P. vivax* infection at Korea University Ansan Hospital, local health centers, and clinics in Gyeonggi and Gangwon provinces, Republic of Korea. Genomic DNA was purified from 200 μL of whole blood by using a QIAamp DNA Blood Mini Kit (QIAGEN, Valencia, CA), according to the manufacturer's protocol. Genomic DNA of *P. vivax* isolates (n = 33) obtained from Thailand (n = 26), Indonesia (n = 3), India (n = 1), Papua New Guinea (n = 1), Western Samoa (n = 1), and Pakistan (n = 1), and nine *P. vivax* laboratory lines (Africa Mauritania, New Guinea, Honduras III, Brazil I, Salvador I, Vietnam IV, Indonesia I, India VII, and Columbia Rio Meta) were used for polymerase chain reaction (PCR).

Amplification and sequencing of target genes. Genomic DNA from 20 isolates from the Republic of Korea and 9 isolates from other locations was used for amplification of the *Pvmsp1p* full-length gene. Primers SeqF1 (5′-TGC ATA TTC ATA CGC GTG TGT-3′) and SeqR8 (5′-GGC TGC CCC TAA CTT AGC A-3′) were designed based on the *Pvmsp1p* sequence of the *P. vivax* Sal I strain. These were used to amplify DNA fragments from 90 basepairs upstream to 80 basepairs downstream of the *Pvmsp1p* coding sequence by using LA Taq DNA polymerase (TaKaRa, Tokyo, Japan). The PCR amplification was performed on a MyCycler Thermal Cycler (Bio-Rad, Hercules, CA) by using the following temperature profile: 94°C for 2 minutes; 35 cycles at 94°C for 30 seconds, 64°C for 30 seconds, 72°C for 6 minutes; and a final extension at 72°C for 10 minutes.

Both strands of the PCR products were directly sequenced by using a series of sequencing forward primers (SeqF1; SeqF2: 5′-ATC AAC CGG AAG AAC TCC CT-3′; SeqF3: 5′-CAA AGG GAG AAG AAA AAA ATG TAC C-3′; SeqF4: 5′-GGT GAG CTA ATC GAA CGG G-3′; SeqF5: 5′-TGG GGC GCA CAT AAC CT-3′; SeqF6: 5′-CCC GTC TAC TCC AAG GAT GTG ATA AG-3′; SeqF7: 5′-TGA AGT GCA ACA CGT GGA AT-3′; SeqF8: 5′-GTG GAC TAC TAC GGG CTA AGG A-3′ and SeqF9: 5′-ATT CTC TAT GCA GAC AAG GAG GTG-3′) and reverse primers (SeqR1: 5′-AAG GCA GGA TTA GAG AGG ACG; SeqR2: 5′-CGC ACG TTT AGG TGG TAG TC-3′; SeqR3: 5′-AGC GTC AAA TCG TGG CAG-3′; SeqR4: 5′-TTC GTG ATG ATC GCG TTG GTT AGC AG-3′; SeqR5: 5′-TCC CCG ATG AAG AAA TAT GC-3′; SeqR6: 5′-ACT GCA GAT GGA TGG TCA TCT-3′; SeqR7: 5′-AAC TGC ATC GCG TCC GTA T-3′; and SeqR8) using an ABI Prism 377 DNA sequencer (Genotech, Seoul, South Korea).

Analysis of the full-length gene sequences showed one highly polymorphic region. This region was amplified by PCR from genomic DNA of 61 samples form the Republic of Korea and 24 samples from other locations, as well as nine laboratory strains, and sequenced. To examine variable tandem repeat regions, as found in the *Pvmsp1p* gene sequence, primers (TR-F: 5′-CCT ACA CGG GAT GGG AGA T-3′ and TR-R: 5′-CGG AGA GCG AGT TCG TGA T-3′) were used to amplify a 200-basepair fragment encompassing this region from 33 worldwide isolates and 9 laboratory lines.

Data analysis. Sequence data were submitted to GenBank under accession numbers GU556592–GU556620. Amino acid sequence alignments were constructed using the MUSCLE program, with manual corrections.[15] The number of nonsynonymous substitutions per nonsynonymous site (dN) and the number of synonymous substitutions per synonymous site (dS) were computed by using the Nei-Gojobori method[16] with the Jukes-Cantor correction, as implemented in the MEGA 4 program.[17] An unrooted tree was constructed by the neighbor-joining method with the Jones-Taylor-Thornton amino acid substitution model,[18] accompanied by bootstrap analysis with 1,000 replicates for the neighbor-joining method and 100 for the maximum parsimony method implemented in PHYLIP version 3.68 after excluding insertions/deletions (indels) and unreliable amino acid sites.[19]

RESULTS

An MSP1P homolog can be found in the *P. vivax* and *P. knowlesi* genome databases, but not in the *P. falciparum*, *P. yoelii*, or *P. berghei* genome databases. To investigate the evolutionary relationship of MSP1P with other MSPs, we searched for *Pvmsp1p* homologs in the available *Plasmodium* genome database and analyzed their relationship with MSP1 by using the distantly related MSP8 and MSP10 sequences as outgroups. A TBLASTN search of the *P. gallinaceum* sequence database (http://www.sanger.ac.uk) was conducted by using the PvMSP1P amino acid sequence as a query. This search identified a contig (28a.d000006175.Contig1) that contained a putative partial sequence of the *Pgmsp1p* gene (encoding the C-terminal end included EGF-like domains) (Figure 2). Based on the BLOSUM matrix, the amino acid sequence identity/similarity of the EGF-like domains to those of PvMSP1P and PkMSP1P were 56/71% and 58/75%, respectively (Figure 3A). The identity/similarity of the N-terminal region of this gene

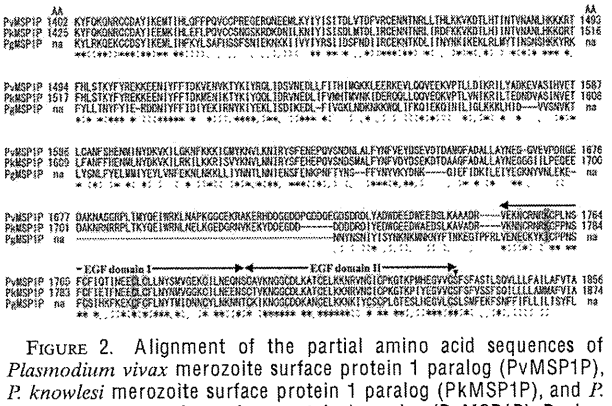

FIGURE 2. Alignment of the partial amino acid sequences of *Plasmodium vivax* merozoite surface protein 1 paralog (PvMSP1P), *P. knowlesi* merozoite surface protein 1 paralog (PkMSP1P), and *P. gallinaceum* merozoite surface protein 1 paralog (PgMSP1P). Dashes indicate deletions. Cys residues with light areas indicate Cys residues conserved among all sequences and those with dark areas and the arrowhead indicate the additional two Cys residues conserved among MSP8, MSP10, MSP1P, and Pf/Pr/PgMSP1 (Figure 3). Asterisks, dots, and colons under the alignment indicate identical, conserved, and semi-conserved substitutions, respectively, based on BLOSUM. The glycosylphosphatidylinositol (GPI) modification site is indicated with arrowhead.

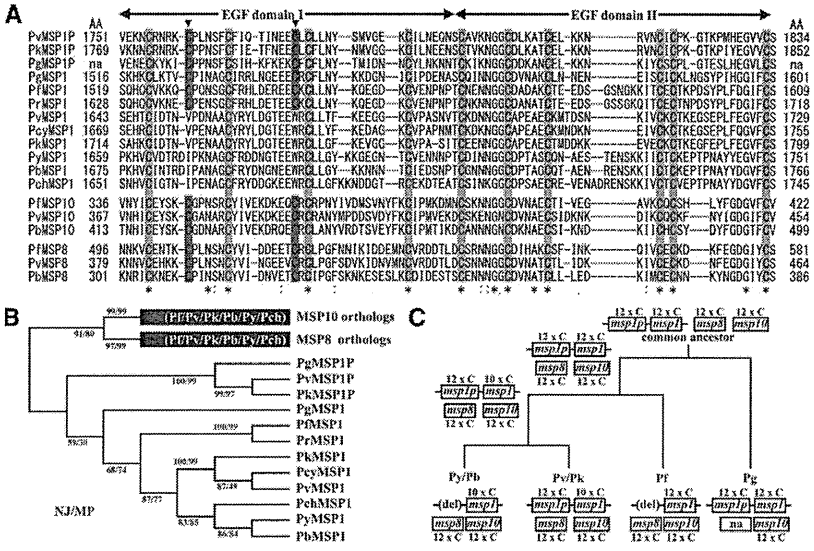

FIGURE 3. Relationship between *Plasmodium vivax* merozoite surface protein 1 paralog (MSP1P) and other *Plasmodium* merozoite surface proteins possessing epidermal growth factor (EGF)–like domains. **A**, Amino acid sequence alignment of the EGF-like domains of *Plasmodium* MSP1, MSP8, MSP10, and MSP1P. Dashes indicate a deletion. Cys residues with light areas indicate Cys residues conserved among all sequences and those with dark areas masks and the arrowhead indicate the additional two Cys residues conserved among MSP8, MSP10, MSP1P, and Pf/Pr/PgMSP1. Asterisks, dots, and colons under the alignment indicate identical, conserved, and semi-conserved substitutions, respectively, based on BLOSUM. **B**, Unrooted dendrograms of the EGF-like region of MSP1, MSP8, MSP10, and MSP1P amino acid sequences. Trees were constructed by the neighbor-joining and maximum parsimony methods using amino acid positions 1759, 1782, 1783, 1784, 1785, 1786, 1787, 1812, 1813, 1814, 1815, 1822, 1823, and 1824 (after *P. vivax* MSP1P amino acid sequence) after excluding indel and unreliable sites. Numbers on branches indicate bootstrap values. **C**, Schematic diagram of the proposed evolutionary history of the *msp1p* gene locus in *Plasmodium* spp. The *msp1p* gene locus was generated by duplication of the *msp1* gene locus in the common ancestor of known *Plasmodium* species. This locus was then deleted in *P. yoelii*, *P. berghei*, and *P. falciparum*. Sequences of *P. falciparum* PfMSP1 (CAA27070), PfMSP8 (PFE0120c) and PfMSP10 (PFF0995c); *P. vivax* PvMSP1 (PVX_099980), PvMSP1P (PVX_099975), PvMSP8 (PVX_097625) and PvMSP10 (PVX_114145); *P. knowlesi* PkMSP1 (PKH_072850) and PkMSP1P (PKH_072840); *P. berghei* PbMSP1 (AAC28871), PbMSP8 (PBANKA_110220) and PbMSP10 (PBANKA_111960); *P. reichenowi* PrMSP1 (CAH10285); *P. gallinaceum* PgMSP1 (CAH10838), PgMSP1P (encoded in 28a.d000006175.Contig1), PgMSP10 (encoded in 28a.d000005716.Contig1); *P. cynomolgi* PcyMSP1 (BAI82251); *P. yoelii* PyMSP1 (PY05748); and *P. chabaudi* PchMSP1 (PCAS_083080) were used.

product to the corresponding region of PvMSP1P (amino acid positions 1,402–1,675) and PkMSP1P (1,425–1,699) were 37/60% and 39/61%, respectively (Figure 2), where the similarity with PgMSP1 was less than 30%. This gene product formed a single clade with Pv/PkMSP1P with high bootstrap values (99–100%; Figure 3B), confirming that this gene was *Pgmsp1p*. Thus, *P. gallinaceum*, *P. vivax*, and *P. knowlesi* have both *msp1* and *msp1p* in their genome and PvMSP1P has weak homology with PvMSP1. This finding, in turn, suggests that the *msp1* and *msp1p* gene loci were generated by a gene duplication event prior to diversification of these parasite species. Because rodent malaria parasite species form a single clade with *P. vivax* and *P. knowlesi*, the lack of a *msp1p* homolog in the *P. yoelii* and *P. berghei* genomes is likely caused by deletion of the *msp1p* gene locus during their evolution. Deletion of this gene locus may also have occurred in *P. falciparum* (Figure 2C).

In a previous study, Carlton and others reported that the PvMSP1P EGF-like domains contained extra two Cys residues absent in PvMSP1 and rodent malaria parasite MSP1, but present in PfMSP1 (Figure 3A).[14] This finding suggested that PvMSP1P might be evolutionarily closer to PfMSP1 than to PvMSP1. However, this appears not to be so for three reasons. First, the dendrogram using EGF-like domains indicated that PvMSP1P formed one clade with PkMSP1P and PgMSP1P and was separated from the MSP1 clade (Figure 3B). Second, beside the EGF-like domains, N-terminal side of the PgMSP1P showed greater similarity to Pv/PkMSP1P (> 60%) than PgMSP1 (< 30%). Third, EGF-like domains of the distantly related MSP8 and MSP10 proteins contain two extra Cys residues, similar to MSP1P and Pf/Pr/PgMSP1. This finding indicates that the common ancestral protein of these MSPs possessed 12 Cys residues (Figure 3A). Collectively, these data suggest that the two Cys sites of the first MSP1 EGF-like domain in *P. vivax*, *P. knowlesi*, *P. yoelii*, and *P. berghei* were substituted with other amino acids during their evolution.

To assess the global genetic diversity of the *Pvmsp1p* gene, we determined the *Pvmsp1p* full-length sequence of 20 isolates of *P. vivax* from the Republic of Korea and 9 strains of *P. vivax* from other locations worldwide. One highly polymorphic glutamate (Glu, E)/glutamine (Gln, Q)-rich region and a polymorphic hepta-peptide motif (SAYSYVS) with number variation (single to triple) were detected. There was no amino acid polymorphism in the EGF-like domains (Figure 1). No diversifying selection was detected, and there was no significant excess of dN over dS.

To determine the repeat variation of the hepta-peptide motif, additional genomic DNA from *P. vivax* worldwide, isolates and laboratory strains was amplified by PCR. All field isolates and laboratory strains had double repeats of this hepta-peptide motif, except for the isolates from Western Samoa (triple repeats) and Pakistan (single repeat). Outside of one E/Q-rich region and the hepta-peptide motif, the sequences were highly conserved with relatively few amino acid substitutions (Table 1).

TABLE 1

Amino acid polymorphisms in the full-length *Plasmodium* merozoite surface protein 1 paralog sequence of *P. vivax* isolates from various locations*

Positions of amino acids	Isolate	
2 3 5 5 7 // 1 1 1 1 1 1 1 1 8 9 0 1 5 // 2 3 3 4 5 5 7 7 9 9 8 7 5 // 3 2 8 0 4 5 0 6 // 2 0 6 4 6 3 3 7	No. (%)	Sources
A R E R S // S R E Q Q E P D		Salvador I (PVX_099975)
. . . . . //	9 (31.0)	South Korea, Thailand, Pakistan, India
. . . . . // . . . . . T .	8 (27.6)	South Korea, Papua New Guinea
. . . . I //	3 (10.3)	South Korea
. . . . I // . . . . . T .	4 (13.8)	South Korea
. . . . I // . . K . . K . .	1 (3.4)	Western Samoa
. . . . . // . . K . . . . E	1 (3.4)	Indonesia
V . . K . //	1 (3.4)	Thailand
. . K . . //	1 (3.4)	Thailand
. Q . . I // N L . K H . . .	1 (3.4)	Thailand
Total	29 (100)	

*// = region included hepta-repeat and E/Q-rich sequences.

Of these substitutions, only the S755I or P1686T (or both) mutations were found in 15 of the isolates from the Republic of Korea and Papua New Guinea, whereas more mutants were found in the worldwide isolates (Table 1).

A short and highly diverse region, composed of Glu and Gln as 3–5 Glu residues, followed by one or several basic E/Q*n* (n = 1–6) units, was found in the *Pvmsp1p* gene. Twenty-one distinguishable allelic types (A1–A21) were identified in 127 isolates (clones), based on a comparison with corresponding regions in the *P. vivax* Sal I strain (Table 2). Type A1 had an identical sequence to that of the Sal I strain, which was found in only two laboratory strains, from Central and South America. Type A2 predominated (33.1%, 42 of 127) in all *P. vivax* samples, and in the Korean (35.8%, 29 of 81), Thai (26.7%, 8 of 30), Pacific (67%, 2 of 3), and African isolates (100%, 1 of 1), which share 96.7% amino acid identity with type A1. The 81 Korean isolates appeared to have limited diversity because only four genotypes (allelic types A2, A7, A20, A21) were found, whereas isolates from other locations worldwide, and laboratory strains, showed 20 allelic types (the exception being A21). Interestingly, type A21 was detected only in Korean isolates (18.5%, 15 of 81).

Polymerase chain reaction amplification resulted in two or three target bands in each of three Thai isolates, which suggested multi-clone infection. To confirm this finding, PCR products of the polymorphic region amplified from these samples was cloned and sequenced. Three types (A2, A16, A20) were detected from the Thai T21 isolate, two (A7, A15) from isolate T25, and two (A19, A20) from isolate T29.

DISCUSSION

We have assessed the evolutionary relationship of the *msp1p* gene with other *msp* genes and propose that a duplication event (*msp1* and *msp1p*) occurred before the diversification of the clades in *P. vivax* and *P. gallinaceum*. This account requires two independent deletions of *msp1p*, one in the rodent lineage (after its divergence from the primate lineage to *P. knowlesi* and *P. vivax*) and another deletion in the lineage to *P. falciparum* (after its divergence from the primate lineage to *P. knowlesi* and *P. vivax*). We also propose that the common ancestor of *P. vivax*, *P. knowlesi*, *P. yoelii*, and *P. berghei* possessed MSP1 that had 12 Cys residues in the first EGF-like domain, and that two Cys sites were substituted to other amino acids during their evolution. We further investigated the genetic diversity of the *Pvmsp1p* gene in isolates from locations worldwide, including the Republic of Korea. We found an E/Q-rich polymorphic region, a hepta repeat region, and several polymorphic sites. However, no diversifying selection was apparent by comparing *d*N and *d*S. Although the molecular data (e.g., size, molecular mass, number, location of Cys residue) were similar to those of PvMSP1, PvMSP1P is not polymorphic and appears to not be under noticeable host immune pressure. However, the repeat-length polymorphism of the E/G-rich region may prove useful as a genetic marker for epidemiologic studies.

High conservation of the double EGF-like domains was also detected in other merozoite surface proteins, such as MSP1 and MSP4. These are involved in putative ligand-receptor interactions during erythrocyte invasion by merozoites.[20,21] Thus, the lack of variation in the C-terminus sequence of PvMSP1P, especially the high conservation of the double EGF-like domains, suggests that these regions play an important role in this process.

The overall nucleotide diversity of *Pvmsp1p* is much lower than that of other *P. vivax* antigens, such as MSP1, MSP3β, and apical membrane antigen 1.[20,22,23] In the PvMSP1P sequences, the E/Q-rich region was shown to be highly polymorphic (21 allelic types in 127 clones/isolates). In the cases of PvMSP1 and Pfs230 (AF269242), the E/Q-rich region was also highly polymorphic and represented the principal source of genetic diversity.[24,25] In a low-complexity region analysis of *Plasmodium*,[26] Gln appeared with a somewhat higher frequency in the repetitive than in the non-repetitive motifs. The E/Q-rich regions and repeat motif of PvMSP1P and Pfs230 were located in a low-complexity region.[27] These low-complexity regions harbor tandem repeats identified in *Plasmodium* and correspond to species-specific and rapidly diverging regions.[26]

This variation in E/Q-rich regions and the number of repeats could be generated by slipped-strand mispairing mechanisms. These result in duplication, deletion, or mutation of certain repeat units.[28,29] The tandem repeat regions of PvMSP1P may result from rapid diversification, which enables the parasite to evade the immune response of the host by antigenic polymorphism.[26]

Finally, the highly polymorphic E/Q-rich region sequence of PvMSP1P might be useful as a genetic marker for studies on the population structure and dynamics of *P. vivax* in malaria-endemic areas.

TABLE 2

Allelic types of the E/Q-rich region of *Plasmodium* merozoite surface protein 1 paralog and geographic prevalence of each *P. vivax* isolate from various locations*

Allelic types	Amino acid sequence variation of E/Q rich region sequence	No. (%) following sources							GenBank accession no.
		South Korea	Thailand	Asia†	Pacific region	Central and South America	Africa	Total	
	1157 1174								
Sal I	EE—EQQQ————————EQEQQEQQQQKK							PVX_099975	
A1	··—·····—·····					2 (50.0)		2 (1.6)	GU556592
A2	··E—····—·····	29 (35.8)	8 (26.6)	2 (25.0)	2 (66.6)		1 (100)	42 (33.1)	GU556607
A3	··EE····—·····		2 (6.7)					2 (1.6)	GU556593
A4	··—····EQ—·····		1 (3.3)					1 (0.8)	GU556594
A5	··—····-QEQQ—·····		1 (3.3)					1 (0.8)	GU556595
A6	··E—····EQEQQ—·····		2 (6.7)					2 (1.6)	GU556596
A7	··—····EQEQQ—·····	18 (22.2)	1 (3.3)					19 (15.0)	GU556597
A8	··E———EQ—·····		5 (16.7)	1 (12.5)				6 (4.7)	GU556617
A9	··E—····EQEQQ———Q-·····				1 (33.3)	1 (25.0)		2 (1.6)	GU556598
A10	··—····—··—·····			1 (12.5)				1 (0.8)	GU556599
A11	··E——— -EQQ—·····					1 (25.0)		1 (0.8)	GU556600
A12	··—····EQEQQ—EQQ-·····			1 (12.5)				1 (0.8)	GU556601
A13	··———EQ——EQ—·····			1 (12.5)				1 (0.8)	GU556616
A14	··E—····EQEQQ—EQQ-·····			1 (12.5)				1 (0.8)	GU556602
A15	··E————————·····		1 (3.3)					1 (0.8)	GU556619
A16	··E—····EQEQQEQEQQ-·····		1 (3.3)					1 (0.8)	GU556618
A17	··—····————EQQ———··		2 (6.7)					2 (1.6)	GU556603
A18	··—····EQEQQQQEQQQ--·····		2 (6.7)	1 (12.5)				3 (2.4)	GU556604
A19	··—····—····———··		2 (6.7)					2 (1.6)	GU556605
A20	··E—····—····———··	19 (23.5)	2 (6.7)					21 (16.5)	GU556611
A21	··E—····EQ———EQQQ····———··	15 (18.5)						15 (11.8)	GU556606
	Total	81 (100)	30‡ (100)	8 (100)	3 (100)	4 (100)	1 (100)	127 (100)	

* Dots and dashes represent identical residues and deletions, respectively.
† Asia except South Korea and Thailand.
‡ Including four clones found in mixed infection from Thailand isolates.

Received July 30, 2010. Accepted for publication October 7, 2010.

Acknowledgment: We thank A. Escalante for providing the *P. vivax* DNA samples of laboratory strain used in this study.

Financial support: This study was supported by National Research Foundation of Korea grant (2009-075103) from the Korean government.

Disclaimer: The views of the authors do not purport to reflect the position of the U.S. Department of the Army or Department of Defense.

Authors' addresses: Yue Wang and Jun-Hu Chen, Department of Parasitology, Kangwon National University College of Medicine, Chuncheon, Gangwon-do 200-701, Republic of Korea and Institute of Parasitic Diseases, Zhejiang Academy of Medical Sciences, Hangzhou 310013, People's Republic of China, E-mails: wangyuerr@yahoo.com.cn and hzjunhuchen@yahoo.com.cn. Osamu Kaneko, Department of Protozoology, Institute of Tropical Medicine, Nagasaki University, 1-12-4 Sakamoto, Nagasaki, Japan, E-mail: okaneko@nagasaki-u.ac.jp. Jetsumon Sattabongkot, Department of Entomology, Armed Forces Research Institute of Medical Science, Bangkok 10400, Thailand, E-mail: JetsumonP@afrims.org. Feng Lu, Department of Parasitology, Kangwon National University College of Medicine, Chuncheon, Gangwon-do 200-701, Republic of Korea and Jiangsu Institute of Parasitic Diseases, Wuxi 214064, People's Republic of China, E-mail: lufeng981@hotmail.com. Jong-Yil Chai, Department of Parasitology and Tropical Medicine, Seoul National University College of Medicine, Seoul, Republic of Korea, E-mail: cjy@snu.ac.kr. Satoru Takeo and Takafumi Tsuboi, Cell-Free Science and Technology Research Center, Ehime University, 3 Bunkyo-cho, Matsuyama, Ehime 790-8577, Japan, E-mails: tsuboi@ccr.ehime-u.ac.jp and stakeo@ccr.ehime-u.ac.jp. Francisco J. Ayala, Department of Ecology and Evolutionary Biology, University of California, Irvine, CA, E-mail: fjayala@uci.edu. Yong Chen, Zhejiang Medical College, Hangzhou 310053, and Zhejiang Academy of Medical Sciences, Hangzhou 310013, People's Republic of China, E-mail: cyong93@yahoo.com.cn. Chae Seung Lim, Department of Laboratory Medicine, College of Medicine, Korea University, Seoul 152-703, Republic of Korea, E-mail: malarim@korea.ac.kr. Eun-Taek Han, Department of Parasitology, Kangwon National University College of Medicine, Chuncheon, Gangwon-do 200-701, Republic of Korea, E-mail: ethan@kangwon.ac.kr.

REFERENCES

1. Price RN, Tjitra E, Guerra CA, Yeung S, White NJ, Anstey NM, 2007. Vivax malaria: neglected and not benign. *Am J Trop Med Hyg 77:* 79–87.
2. Mueller I, Galinski MR, Baird JK, Carlton JM, Kochar DK, Alonso PL, del Portillo HA, 2009. Key gaps in the knowledge of *Plasmodium vivax*, a neglected human malaria parasite. *Lancet Infect Dis 9:* 555–566.
3. Herrera S, Corradin G, Arevalo-Herrera M, 2007. An update on the search for a *Plasmodium vivax* vaccine. *Trends Parasitol 23:* 122–128.
4. Udomsangpetch R, Kaneko O, Chotivanich K, Sattabongkot J, 2008. Cultivation of *Plasmodium vivax*. *Trends Parasitol 24:* 85–88.
5. Galinski MR, Barnwell JW, 2008. *Plasmodium vivax*: who cares? *Malar J 7 (Suppl 1):* S9.
6. Black CG, Barnwell JW, Huber CS, Galinski MR, Coppel RL, 2002. The *Plasmodium vivax* homologues of merozoite surface proteins 4 and 5 from *Plasmodium falciparum* are expressed at different locations in the merozoite. *Mol Biochem Parasitol 120:* 215–224.
7. Perez-Leal O, Sierra AY, Barrero CA, Moncada C, Martinez P, Cortes J, Lopez Y, Torres E, Salazar LM, Patarroyo MA, 2004. *Plasmodium vivax* merozoite surface protein 8 cloning, expression, and characterisation. *Biochem Biophys Res Commun 324:* 1393–1399.
8. Perez-Leal O, Sierra AY, Barrero CA, Moncada C, Martinez P, Cortes J, Lopez Y, Salazar LM, Hoebeke J, Patarroyo MA, 2005. Identifying and characterising the *Plasmodium falciparum* merozoite surface protein 10 *Plasmodium vivax* homologue. *Biochem Biophys Res Commun 331:* 1178–1184.
9. de Oliveira CI, Wunderlich G, Levitus G, Soares IS, Rodrigues MM, Tsuji M, del Portillo HA, 1999. Antigenic properties of the merozoite surface protein 1 gene of *Plasmodium vivax*. *Vaccine 17:* 2959–2968.
10. Udagama PV, Gamage-Mendis AC, David PH, Peiris JS, Perera KL, Mendis KN, Carter R, 1990. Genetic complexity of *Plasmodium vivax* parasites in individual human infections analyzed with monoclonal antibodies against variant epitopes on a single parasite protein. *Am J Trop Med Hyg 42:* 104–110.
11. Putaporntip C, Jongwutiwes S, Sakihama N, Ferreira MU, Kho WG, Kaneko A, Kanbara H, Hattori T, Tanabe K, 2002. Mosaic organization and heterogeneity in frequency of allelic recombination of the *Plasmodium vivax* merozoite surface protein-1 locus. *Proc Natl Acad Sci U S A 99:* 16348–16353.
12. Cui L, Escalante AA, Imwong M, Snounou G, 2003. The genetic diversity of *Plasmodium vivax* populations. *Trends Parasitol 19:* 220–226.
13. Gilson PR, Nebl T, Vukcevic D, Moritz RL, Sargeant T, Speed TP, Schofield L, Crabb BS, 2006. Identification and stoichiometry of glycosylphosphatidylinositol-anchored membrane proteins of the human malaria parasite *Plasmodium falciparum*. *Mol Cell Proteomics 5:* 1286–1299.
14. Carlton JM, Adams JH, Silva JC, Bidwell SL, Lorenzi H, Caler E, Crabtree J, Angiuoli SV, Merino EF, Amedeo P, Cheng Q, Coulson RM, Crabb BS, Del Portillo HA, Essien K, Feldblyum TV, Fernandez-Becerra C, Gilson PR, Gueye AH, Guo X, Kang'a S, Kooij TW, Korsinczky M, Meyer EV, Nene V, Paulsen I, White O, Ralph SA, Ren Q, Sargeant TJ, Salzberg SL, Stoeckert CJ, Sullivan SA, Yamamoto MM, Hoffman SL, Wortman JR, Gardner MJ, Galinski MR, Barnwell JW, Fraser-Liggett CM, 2008. Comparative genomics of the neglected human malaria parasite *Plasmodium vivax*. *Nature 455:* 757–763.
15. Edgar RC, 2004. MUSCLE: multiple sequence alignment with high accuracy and high throughput. *Nucleic Acids Res 32:* 1792–1797.
16. Nei M, Gojobori T, 1986. Simple methods for estimating the numbers of synonymous and nonsynonymous nucleotide substitutions. *Mol Biol Evol 3:* 418–426.
17. Tamura K, Dudley J, Nei M, Kumar S, 2007. MEGA4: Molecular Evolutionary Genetics Analysis (MEGA) software version 4.0. *Mol Biol Evol 24:* 1596–1299.
18. Jones DT, Taylor WR, Thornton JM, 1992. The rapid generation of mutation data matrices from protein sequences. *Comput Appl Biosci 8:* 275–282.
19. Felsenstein J, 1993. *PHYLIP (Phylogeny Inference Package) Version 3.5c*. Seattle, WA: Department of Genetics, University of Washington.
20. Thakur A, Alam MT, Sharma YD, 2008. Genetic diversity in the C-terminal 42 kDa region of merozoite surface protein-1 of *Plasmodium vivax* (PvMSP-1(42)) among Indian isolates. *Acta Trop 108:* 58–63.
21. Putaporntip C, Jongwutiwes S, Ferreira MU, Kanbara H, Udomsangpetch R, Cui L, 2009. Limited global diversity of the *Plasmodium vivax* merozoite surface protein 4 gene. *Infect Genet Evol 9:* 821–826.
22. Thakur A, Alam MT, Bora H, Kaur P, Sharma YD, 2008. *Plasmodium vivax*: sequence polymorphism and effect of natural selection at apical membrane antigen 1 (PvAMA1) among Indian population. *Gene 419:* 35–42.
23. Rayner JC, Huber CS, Feldman D, Ingravallo P, Galinski MR, Barnwell JW, 2004. *Plasmodium vivax* merozoite surface protein PvMSP-3 beta is radically polymorphic through mutation and large insertions and deletions. *Infect Genet Evol 4:* 309–319.
24. Leclerc MC, Menegon M, Cligny A, Noyer JL, Mammadov S, Aliyev N, Gasimov E, Majori G, Severini C, 2004. Genetic diversity of *Plasmodium vivax* isolates from Azerbaijan. *Malar J 3:* 40.
25. Niederwieser I, Felger I, Beck HP, 2001. Limited polymorphism in *Plasmodium falciparum* sexual-stage antigens. *Am J Trop Med Hyg 64:* 9–11.
26. Brocchieri L, 2001. Low-complexity regions in *Plasmodium* proteins: in search of a function. *Genome Res 11:* 195–197.
27. Aurrecoechea C, Brestelli J, Brunk BP, Dommer J, Fischer S, Gajria B, Gao X, Gingle A, Grant G, Harb OS, Heiges M, Innamorato F, Iodice J, Kissinger JC, Kraemer E, Li W, Miller JA, Nayak V, Pennington C, Pinney DF, Roos DS, Ross C, Stoeckert CJ Jr, Treatman C, Wang H, 2009. PlasmoDB: a functional genomic database for malaria parasites. *Nucleic Acids Res 37:* D539–D543.
28. Pizzi E, Frontali C, 2001. Low-complexity regions in *Plasmodium falciparum* proteins. *Genome Res 11:* 218–229.
29. Tanabe K, Sakihama N, Kaneko A, 2004. Stable SNPs in malaria antigen genes in isolated populations. *Science 303:* 493.

Vaccine 29 (2011) 2720–2726

Contents lists available at ScienceDirect

Vaccine

journal homepage: www.elsevier.com/locate/vaccine

Adenovirus-vectored *Plasmodium vivax* ookinete surface protein, Pvs25, as a potential transmission-blocking vaccine

Takeshi Miyata[a], Tetsuya Harakuni[a], Hideki Sugawa[a,b], Jetsumon Sattabongkot[c], Aki Kato[d], Mayumi Tachibana[e], Motomi Torii[e], Takafumi Tsuboi[d], Takeshi Arakawa[a,f,*]

[a] *Molecular Microbiology Group, Department of Tropical Infectious Diseases, COMB, Tropical Biosphere Research Center, University of the Ryukyus, 1 Senbaru, Nishihara, Okinawa 903-0213, Japan*
[b] *AMBiS Corporation, 2013 Ozato, Nanjyo, Okinawa 901-1202, Japan*
[c] *Department of Entomology, Armed Forces Research Institute of Medical Sciences, Bangkok 10400, Thailand*
[d] *Cell-Free Science and Technology Research Center, Ehime University, 3 Bunkyo-cho, Matsuyama, Ehime 790-8577, Japan*
[e] *Department of Molecular Parasitology, Ehime University, Graduate School of Medicine, Shitsukawa, Toon, Ehime 791-0295, Japan*
[f] *Division of Host Defense and Vaccinology, Graduate School of Medicine, University of the Ryukyus, 207 Uehara, Nishihara, Okinawa 903-0215, Japan*

ARTICLE INFO

Article history:
Received 10 September 2010
Received in revised form
29 December 2010
Accepted 21 January 2011
Available online 11 February 2011

Keywords:
Malaria transmission-blocking vaccine
Human adenovirus

ABSTRACT

Adjuvants or delivery vehicles are essential components to expedite malaria vaccine development. In this study, replication-defective human adenovirus serotype 5 (rAd) was genetically engineered to express the *Plasmodium vivax* ookinete surface protein (OSP), Pvs25 (AdPvs25). BALB/c mice immunized with the AdPvs25 through various routes including intramuscular, subcutaneous and intranasal routes were analyzed for induction of antigen-specific transmission-blocking immunity. Parenteral but not mucosal immunization induced high serum immunoglobulin G (IgG) responses specific to *P. vivax* ookinetes isolated from *P. vivax* volunteer patients from Thailand. The membrane feeding assay revealed that antisera conferred a transmission blockade of up to 99% reduction in the average oocyst numbers per mosquito, while immunization with a rAd expressing Pfs25 from *Plasmodium falciparum*, a homolog of Pvs25, conferred only a background level of blockade, suggesting that a species-specific transmission-blocking immunity was induced. Vaccine efficacy of AdPvs25 was slightly higher than to a recombinant Pvs25 protein mixed with aluminum hydroxide, but less efficacious than the protein emulsified with incomplete Freund's adjuvant. This study, the first preclinical evaluation of adenovirus-vectored malaria OSPs, implicates a potential inclusion of malaria transmission-blocking vaccine antigens in viral vector systems.

1. Introduction

Malaria is one of the most serious infectious diseases with high mortality and morbidity in large areas of tropical regions of the world. There were estimated 189–327 million cases and 881,000 malaria deaths in 2006 [1]. The majority of victims of malaria are children in sub-Saharan Africa. Implementation of various control measures including drug therapy and insecticide-treated bednets have made a substantial contribution to reduction of malaria cases over the past decades; however, these control measures are not sufficient partly due to the emergence of parasites resistant to antimalarial drugs and mosquito strains resistant to insecticides, and hence new prevention tools need to be developed for local elimination and the ultimate eradication of the disease [2–4]. The development of effective and affordable vaccines is therefore believed to benefit global public health by closing the gap left by the current malaria intervention measures [5].

Several promising vaccine candidates have been intensively investigated [6,7], such as those targeting sporozoite [8], hepatic and erythrocytic stages [9], which are designed to prevent infection and to reduce disease severity. On the other hand, transmission-blocking vaccines (TBVs) that target the sexual stage, in which the parasite undergoes sporogonic development in anopheline mosquitoes, prevent parasite transmission in the mosquito [10–12]. TBVs induce antibodies that react with the ookinete surface proteins (OSPs) of malaria parasites within the mosquito midgut, and as such they do not directly protect vaccinated individuals from infection. They could however contribute to elimination of the disease by lowering the parasite transmission

* Corresponding author at: Molecular Microbiology Group, Department of Tropical Infectious Diseases, COMB, Tropical Biosphere Research Center, University of the Ryukyus, 1 Senbaru, Nishihara, Okinawa 903-0213, Japan.
Tel.: +81 98 895 8974; fax: +81 98 895 8974.
E-mail address: tarakawa@comb.u-ryukyu.ac.jp (T. Arakawa).

0264-410X/$ – see front matter © 2011 Elsevier Ltd. All rights reserved.
doi:10.1016/j.vaccine.2011.01.083

frequency below the threshold at which the parasite can maintain its life cycle [2,13,14]. Additionally, TBVs, if combined with vaccines targeting other infection stages, could prevent transmission of escape mutants that emerge during infection. Therefore, TBVs might function as a "safety net" for pre-erythrocytic and erythrocytic vaccines, as well as other non-vaccine interventions.

Plasmodium falciparum causes the highest mortality rates among the four *Plasmodium* species known to infect humans; however *Plasmodium vivax*, the second most prevalent malaria species, causes 80–300 million clinical cases every year [15], has the highest morbidity and is a major cause of recurrent malaria. Its clinical manifestations range from asymptomatic to severe diseases that in some cases lead to death. Additionally, an increase in the number of severe cases of *P. vivax* infection casts doubts regarding what was thought to be its relatively benign nature [16]. This species is therefore an important target of malaria control efforts [5,13–15,17]. Furthermore, because global malaria eradication is the ultimate goal, the value of developing vaccines against *P. vivax* can no longer be underestimated [5,13–15,17].

The majority of malaria vaccine candidate antigens currently under preclinical and clinical evaluation are recombinant in origin [6,7], and therefore they are only marginally immunogenic by themselves. This has been demonstrated to be true for the two *P. vivax* candidate vaccine antigens recently tested in clinical trials, the circumsporozoite protein (CSP) [13,18] and Pvs25 OSP [13,19,20]. Therefore, appropriate adjuvant formulations or employment of delivery systems seem to be extremely important in inducing an optimal antiparasite immune response.

Replication-defective human adenovirus has been intensively evaluated for the delivery of foreign genes in gene therapy and for vaccine development against infectious diseases including malaria [21–23]. The ability to induce both cell-mediated and humoral immunities as well as a long-lasting memory T cell response are generally considered advantages of the viral vector systems in vaccine development against malaria [21,23,24]. Those immunities are important to confer solid protection against infection [25]. Attenuated adenovirus has been used for US military recruits to prevent respiratory infection [23,26], therefore safety issues may not be a serious concern for this viral vector system. *P. falciparum* antigens at the pre-erythrocytic stage such as CSP and liver-stage antigen-1 (LSA1), and antigens at the erythrocytic stage such as apical membrane antigen-1 (AMA1) and merozoite surface protein-1 (MSP1) are being tested in clinical trials as adenovirus-vectored antigens [7,23].

Since TBVs require efficient antibody-inducing capacity [10–12,27–30], we therefore hypothesized that the adenovirus vector system is beneficial for this purpose. In this study we evaluated potential application of a replication-defective human adenovirus serotype 5 to induce transmission-blocking immunity against *P. vivax* malaria. The vaccine efficacy of the induced mouse antisera was evaluated by a membrane-feeding assay using field strains of parasites obtained from *P. vivax* volunteer patients in Thailand.

2. Materials and methods

2.1. Immunization with a recombinant adenovirus expressing Pvs25

AdPvs25 is a replication-defective human adenovirus serotype 5, expressing the Pvs25 gene under the regulation of the cytomegalovirus enhancer and promoter [31]. Genetic engineering of AdPvs25 was conducted based on a COS-TPC method, according to the manufacturer's instructions (TAKARA Bio, Otsu, Japan). Recombinant Pvs25 (rPvs25) protein expressed and purified from the methylotrophic yeast *Pichia pastoris* [27] was used to comparatively evaluate immunogenicity of AdPvs25.

Eight-week-old female BALB/c mice were purchased from Japan SLC (Shizuoka, Japan), and housed in a special pathogen-free environment in our research institute. Mice were immunized four times at weeks 0, 3, 5 and 7 *via* subcutaneous (s.c.; 100 μl at a single injection site), intramuscular (i.m.; 50 μl at two injection sites), intranasal (i.n.; 15 μl into each nostril), or intragastric (i.g.; 200 μl) route with 5.1×10^9 plaque forming units/ml of AdPvs25, or three times at weeks 0, 2 and 4 *via* the s.c. route with 30 μg of the rPvs25 protein alone, or with incomplete Freund's adjuvant (IFA; Difco Laboratories, Detroit, MI, USA) or aluminum hydroxide (Alum; Pierce, Rockford, IL, USA) as controls.

All animal experimental protocols used in this study were approved by the Institutional Animal Care and Use Committee of the University of the Ryukyus, and the experiments were conducted according to the Ethical Guidelines for Animal Experiments of the University of the Ryukyus.

2.2. ELISA for antibody titer determination

Mouse antisera were collected 1–2 weeks after the last immunization (week 8 or 6 for AdPvs25 or rPvs25 protein, respectively), and Pvs25-specific serum IgG was analyzed by ELISA as described previously [27–30]. Briefly, the ELISA plates (Sumilon; Sumitomo Bakelite Co., Ltd., Tokyo, Japan) were coated with 5 μg/ml of rPvs25 in bicarbonate buffer overnight at 4 °C and blocked with 1% (w/v) bovine serum albumin (BSA) in phosphate buffered saline (PBS) for 2 h at 37 °C. Two-fold serial dilutions of the antisera, commencing with an initial 50-fold dilution with 0.5% (w/v) BSA in PBS, were applied to wells (2 h, 37 °C). Anti-mouse IgG conjugated to alkaline phosphatase (1/4000; Sigma–Aldrich, St. Louis, MO, USA) was added to the wells and incubated for 2 h at 37 °C, before its substrate *p*-nitrophenylphosphate (Bio-Rad Laboratories, Inc., Redmond, WA, USA) was applied for 20 min at 37 °C and the absorbance at 415 nm (OD_{415}) was read on a microplate reader (Bio-Rad). The plates were washed twice with PBS containing 0.05% Tween-20 (PBS-T) and once with PBS between each incubation step. The antibody titer was defined as the serum dilution that gave an OD_{415} value equal to 0.1, or as the serum dilution where a one magnitude higher dilution gave an OD_{415} value less than 0.1.

2.3. Mosquito membrane feeding assay

The membrane feeding assay was conducted as described previously [27–29]. Briefly, peripheral blood was collected, with written informed consent, from *P. vivax* volunteer patients who came to a malaria clinic in the Mae Sod district in the Tak province of northwestern Thailand. Plasma was removed from the collected blood. Single species infection with *P. vivax* was confirmed by Giemsa stain prior to the assay. The vaccine-induced mouse antisera were mixed with an equal volume of heat-inactivated human AB serum obtained from malaria-naïve volunteers. Then, the mouse antisera and the human AB serum mixture was added to the parasitized blood cells obtained from the patients (1:1 v/v ratio), and incubated for 15 min at room temperature. The mixture was applied to a membrane feeding apparatus kept at 37 °C to feed *Anopheles dirus* A mosquitoes (Bangkok colony, Armed Forces Research Institute of Medical Sciences) for 30 min. Fully engorged mosquitoes were maintained for a week in an insectary kept at 26 °C. For each test sample, 20 mosquitoes were analyzed to count the number of oocysts that had developed in the midgut.

Human subject research conducted in this study was reviewed and approved by the Ethics Committee of the Thai Ministry of Public Health and the Institutional Review Board of the Walter Reed Army Institute of Research.